TECHNICAL REVIEW

No.26 / September 2026

Technical Review

Willpower to Empower Generations

Event

MAPNA GROUP
MAPNA Turbine Engineering
and Manufacturing Company

TECHNICAL REVIEW

Acknowledgment

We would like to express our sincere appreciation to **Dr. Mohammad Owliya** for his valuable role in initiating the Technical Review and for his encouragement, guidance, and continued support since its inception, which have contributed significantly to the development of this publication.

Cover Page:
MGT-75 Gas Turbine: Official Unveiling

Editorial

Dear Colleagues, Partners and Professionals,

In today's dynamic industrial landscape, staying ahead means not just meeting standards, but redefining them. At the heart of MAPNA Turbine's mission lies a strong commitment to innovation and deep customer partnership, driving us to continuously enhance our capabilities and solutions. It is in this context, and with great pleasure, that we present to you, our valued readers, a brief account of a few recent technological achievements in this edition of TUGA Technical Review.

The first article presents the MGT-75, Iran's first F-class heavy-duty gas turbine, designed and developed entirely in-house to improve efficiency, reliability, and environmental performance. Comprehensive aerodynamic, thermal, structural, and dynamic analyses confirmed the performance and durability of its major components. This gas turbine demonstrates MAPNA's capability in advanced gas-turbine technology and provides a strong platform for future developments.

TUGA's development of centrifugal compressors for a case-study gas storage project is outlined in the second article. The compressors underwent mechanical, performance, and leakage tests, with the results confirming their reliability, integrity, and suitability for critical gas-storage applications. The project strengthens Iran's domestic capabilities in compressor technology and supports energy security and efficient gas management.

The third article highlights an automated approach for on-site gas turbine performance tests when factory test data are not available. The proposed method combines data processing, steady-state identification, thermodynamic calculations, and performance analysis to provide consistent results under different operating conditions. This methodology improves testing efficiency, accuracy, and traceability.

A three-dimensional CFD-based method for estimating axial thrust in heavy-duty gas turbines is introduced in the fourth article. By accounting for aerodynamic and secondary-air forces, the approach provided a more detailed assessment of thrust and was successfully validated against field measurements, improving thrust-bearing design and turbine reliability.

The last article outlines miniature testing techniques for evaluating the condition and remaining life of turbine components with minimal material removal and no significant damage. The techniques provide useful information on material degradation and mechanical properties, offering a practical approach to component life assessment, maintenance planning, and life extension.

Please join us in exploring a detailed account of these subjects in this issue of the Technical Review.

Respectfully,

Roohollah Jabery,

Vice President for Engineering and R&D

R Jabery

MAPNA Turbine Company (TUGA)

September 2026

Contents

Design and Development of Iran's First F-Class Heavy-Duty Gas Turbine

1

Babaei, Masoume
Yoosefi, Elahe
Mostafavi, SeyedMilad
Bagheri, Yousef

MAPNA Turbine Engineering & Manufacturing Co. (TUGA)

Introduction

Meeting the increasing energy demand driven by rapid industrial and technological development has intensified the need for advanced F-class gas turbines, which represent one of the most efficient power generation technologies. Besides their strategic role in electricity generation, developing the technologies required for these turbines is essential for maintaining competitiveness in the global energy market.

In response, MAPNA Group has focused on developing the design and manufacturing capabilities of F-class gas turbines to improve efficiency, increase power output and reliability, reduce production and maintenance costs, and enhance overall performance. Compared with E-class turbines, F-class machines operate at higher turbine inlet temperatures, employ advanced cooling technologies, and feature higher compressor pressure ratios and efficiencies.

The outcome of these development efforts is the MGT-75, MAPNA Group's and Iran's first F-class heavy-duty gas turbine designed and developed entirely in-house. Designed for both simple-cycle and combined-cycle applications, the MGT-75 combines advanced aerodynamic, thermal, and mechanical design solutions to achieve high efficiency, increased power output, and enhanced reliability while reducing greenhouse gas and pollutant emissions.

This paper presents the overall design of the MGT-75 gas turbine, including its compressor, combustion system, turbine, rotor, and casings, with emphasis on the engineering considerations underlying component design and system integration.

Overall Configuration and Description of MGT-75

Based on the experience gained from the design and manufacturing of the MGT-70 turbine, the MGT-75 development process was conducted through a structured program including conceptual design, engineering, manufacturing, validation, and commissioning phases, as illustrated in Figures 1 and 2.

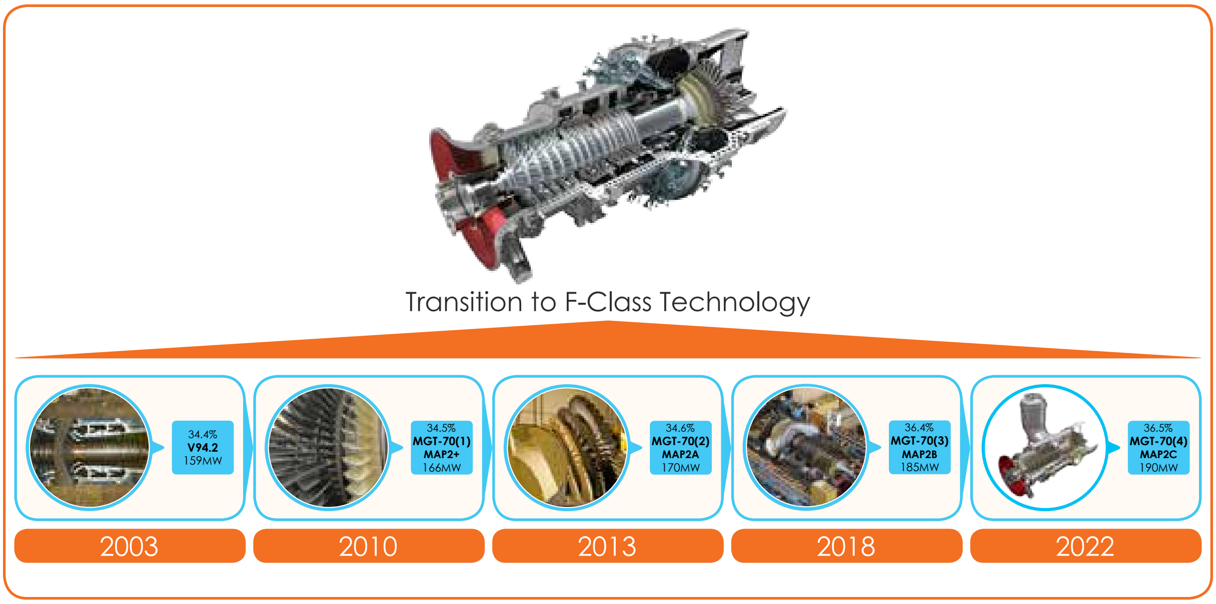

Figure 1- Development and Design Pathway of MAPNA Group MGT-75 Gas Turbine

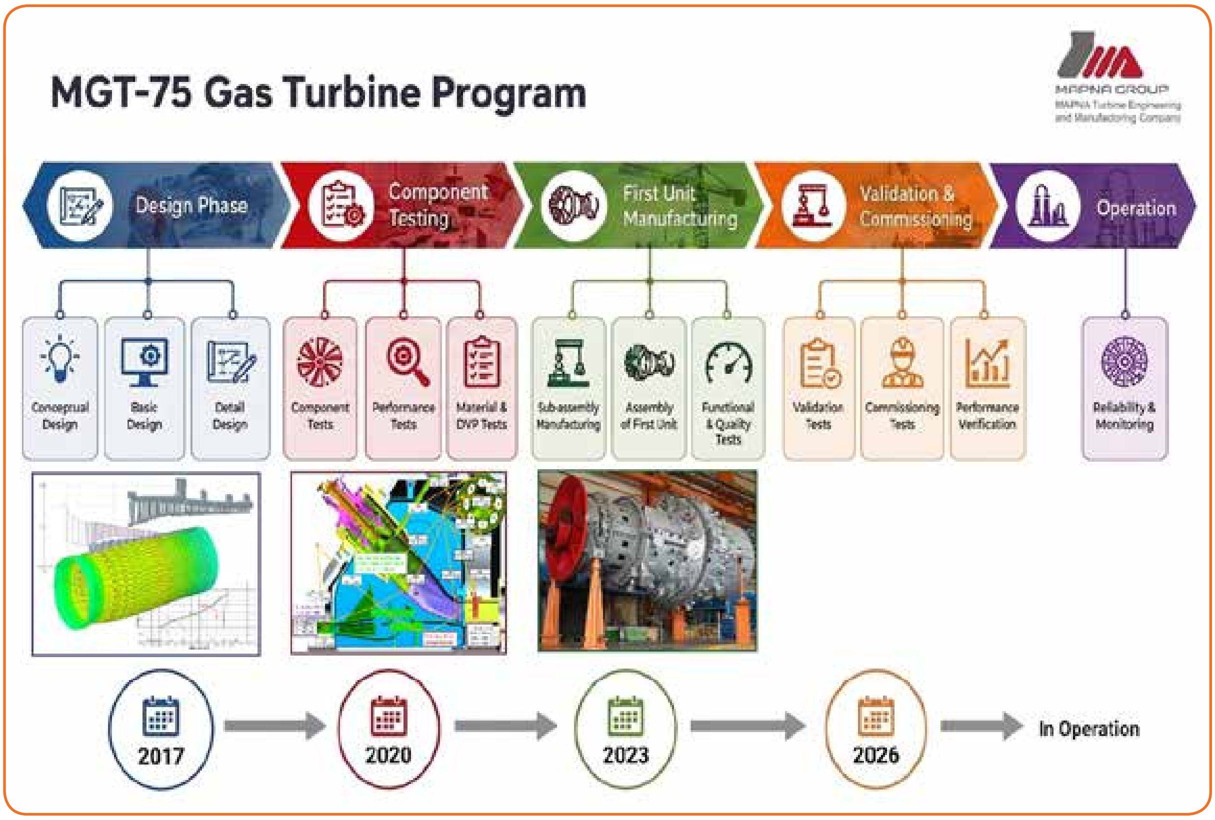

Figure 2- MGT-75 Development Project Timeline and Major Milestones

The MGT-75 gas turbine is designed for both base-load and peak-load applications and can be integrated into simple-cycle and combined-cycle power plants. The machine employs a can-annular combustion system, horizontally split casing architecture, and advanced design solutions to enhance performance, reliability, and maintainability. The main design features and engineering considerations of the MGT-75 are summarized as follows:

- Compressor with optimized flow distribution and variable inlet guide vanes.
- Can-annular combustion system equipped with a dry low-NOx burner, capable of hydrogen firing.
- Combustion system with 16 burners, double layer combustion liners, and film cooled transition piece.
- Horizontally-split casing.
- Rotor disks interlocked and centered by Hirth serrations and axially fixed by a central tie bolt.
- Turbine with advanced cooling technology, thermal barrier blade coatings, and film cooling of blade airfoils.
- Two-bearing rotor design for easy alignment.
- Reliable fast start and appealing ramp-up sequences.
- Design features that facilitate maintenance.
- Manholes that permit access to the combustion chamber and hot gas path for inspection without the need to open the turbine casing.

Based on these characteristics, the technological position of the MGT-75 among E-class and F-class gas turbines can be evaluated in terms of Turbine Inlet Temperature (TIT) and efficiency, as illustrated in Figure 3.

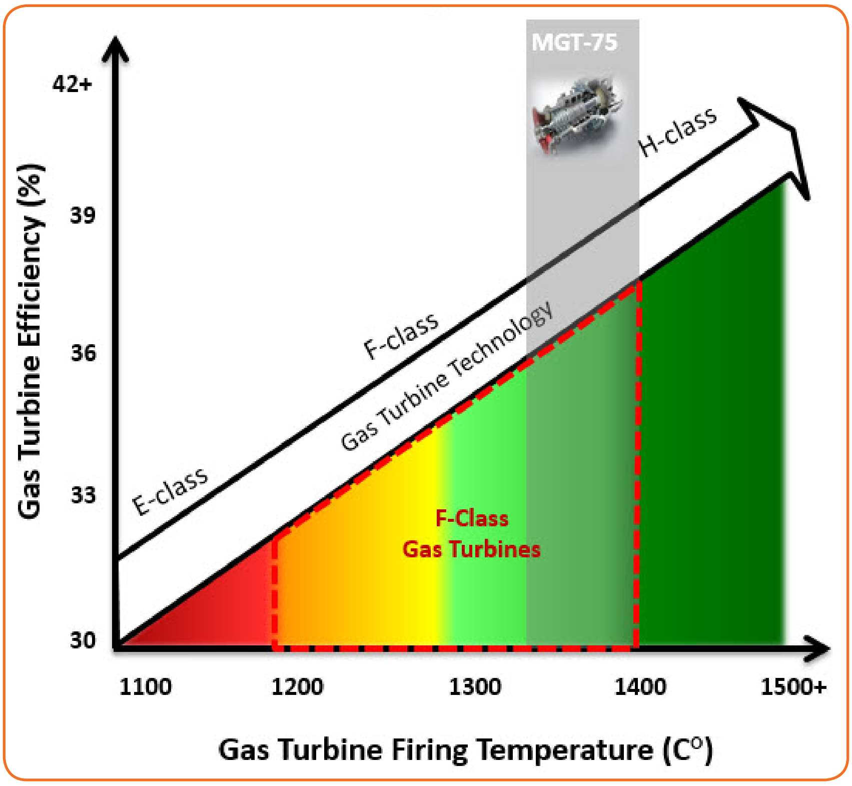

Figure 3- Position of the MGT-75 Gas Turbine among the E-Class and F-Class Gas Turbines

Table 1 summarizes the principal technical specifications of the MGT-75 under ISO conditions, and Figure 4 shows the overall configuration of the gas turbine.

Table 1- Main specifications (ISO Conditions*)

1	Gas Turbine Type	F-Class
2	GT Power at Generator (MW)	222
3	GT Efficiency	39.1%
4	Turbine Exhaust Temperature (°C)	571
5	Pressure Ratio	18:1
6	Heat Rate (kJ/kWh)	9207
7	Exhaust Mass Flow Rate (kg/s)	559
8	Compressor	Axial 16 Stages
9	Combustor	16 Cans
10	Turbine	Axial 4 stages

*(Altitude = 0 m, T_{amb} = 15 °C, RH = 60%, InLoss = 0 mbar, ExLoss = 0 mbar, PF = 0.85, Fuel Gas = Methane)

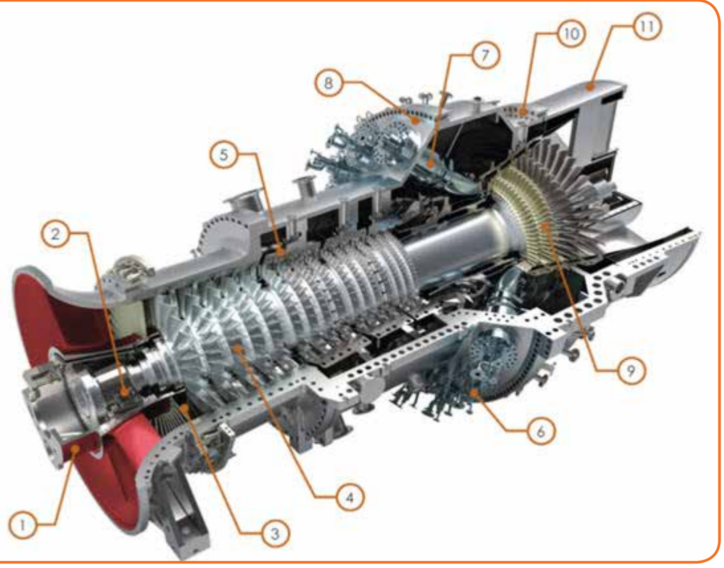

Figure 4- Configuration and Arrangement of MGT-75 Major Components

The following sections provide an overview of the design and development of the MGT-75 major components.

Compressor Section

The development of the high-pressure axial compressor followed a structured engineering process comprising three phases: conceptual, basic, and detailed design.

During the conceptual design phase, the main thermodynamic targets and compressor configuration were established through cycle analysis and preliminary compressor studies. The number of stages, mass flow rate, and overall pressure ratio were determined to satisfy the gas turbine performance requirements while maximizing the use of existing machinery. Preliminary rotor configuration and material selection were also defined based on the expected aerodynamic and mechanical loads.

In the basic design phase, the conceptual design was refined through iterative aerodynamic and structural analyses. One-dimensional mean-line and two-dimensional streamline-curvature methods were used to define the flow path and annulus geometry, followed by the selection of blade numbers for each rotor and stator row. The resulting blade configuration was evaluated using CFD simulations. Simultaneously, comprehensive structural analyses, including blade root design and stress evaluation, verified the mechanical integrity of the compressor. Cooling-air extraction requirements were determined through iterative aerodynamic, structural, and combustor interface assessments, leading to the finalization of the basic compressor architecture.

The detailed design phase focused on manufacturing readiness through high-fidelity 2D and 3D blade optimization to reduce aerodynamic losses and improve off-design performance. Multi-stage CFD simulations validated the internal flow field, while detailed structural, modal, and fatigue analyses confirmed the integrity of the blades and disks. After satisfying all aerodynamic, thermal, and mechanical requirements, the compressor design successfully completed the final design review.

The final design is a 16-stage high-pressure axial compressor with a variable Inlet Guide Vane (IGV) and an overall pressure ratio of 18:1, specifically developed for the MGT-75 gas turbine. The compressor casing consists of four compressor carriers with a horizontally split configuration, facilitating on-site maintenance without complete gas turbine disassembly. The resulting pressure distribution is shown in Figure 5, while the overall mechanical arrangement of the compressor is presented in Figure 6. Photographs of the manufactured compressor carriers are presented in Figure 7.

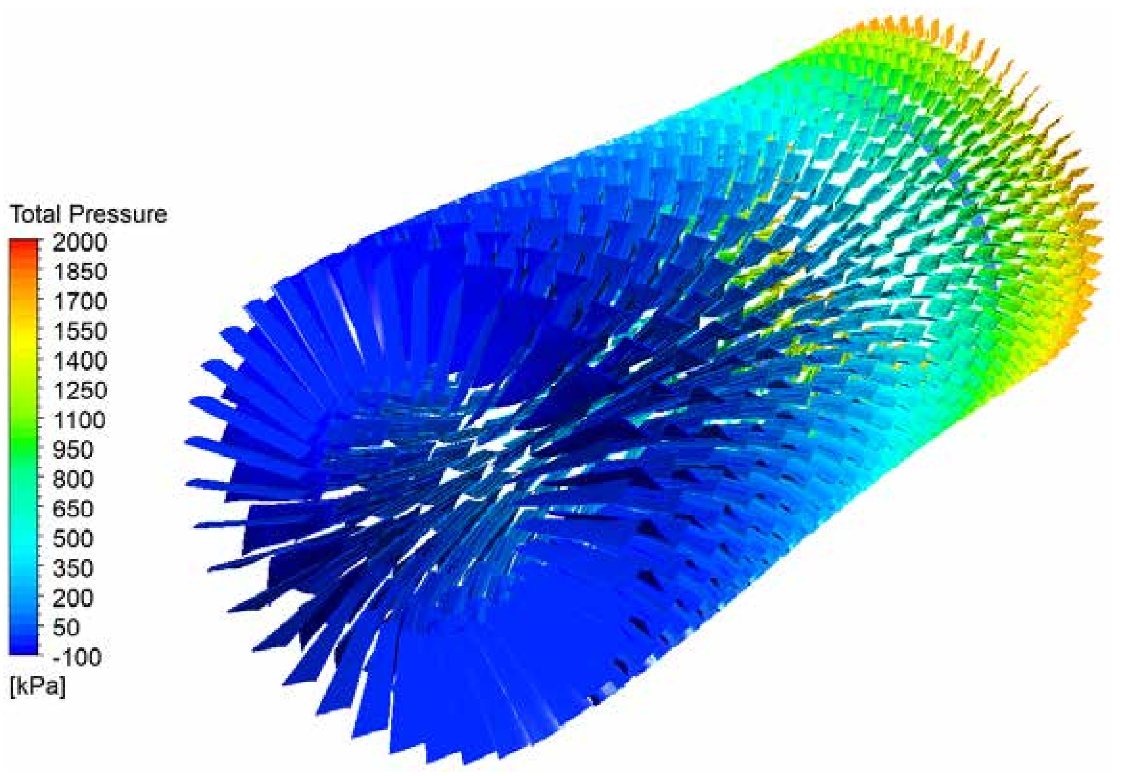

Figure 5- Pressure Distribution in the Compressor Section of MGT-75 Gas Turbine

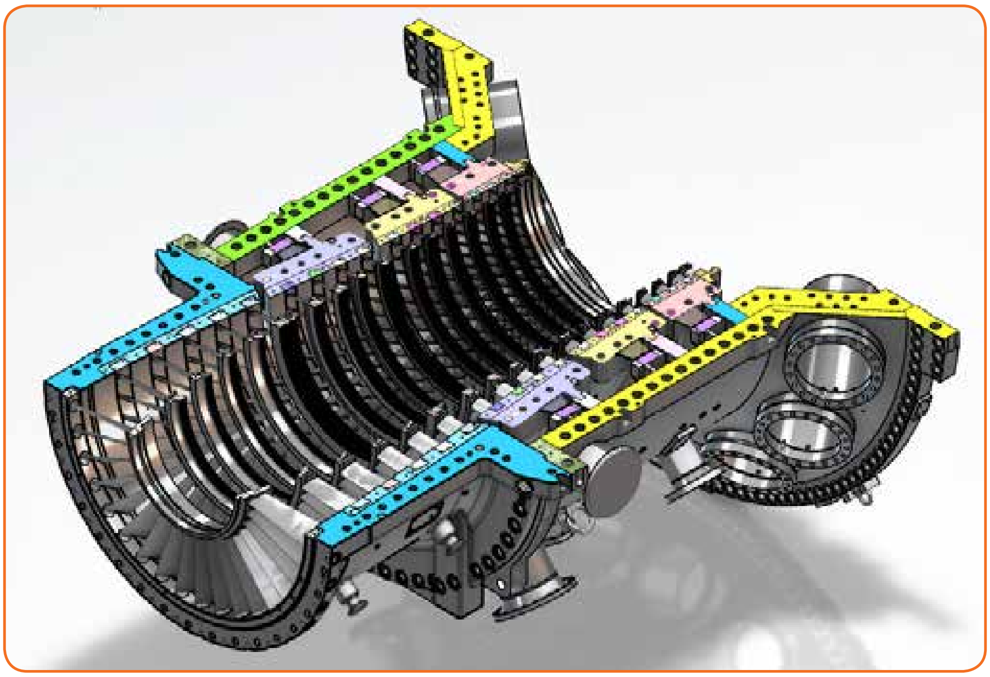

Figure 6- Mechanical Arrangement of the MGT-75 Compressor Section

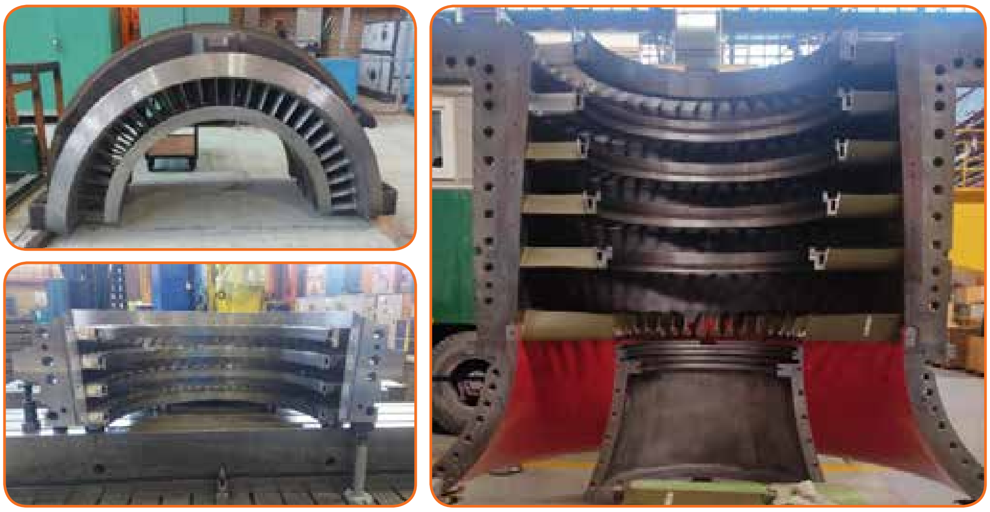

Figure 7- Manufactured MGT-75 Compressor Carriers

In addition to supplying compressed air, the compressor incorporates three blow-off lines to maintain stable operation during start-up and shutdown. Two blow-off ports are located at stage 5 and one at stage 9, with pneumatically actuated valves directing the discharged air to the exhaust diffuser. Furthermore, cooling air is extracted from selected compressor stages and delivered through annular passages between the tie bolt and disks to provide effective cooling of the turbine stationary and rotating components.

Combustion System

For the MGT-75 turbine, different combustion chamber configurations were evaluated considering their advantages, limitations, and industrial applications. Based on this assessment, the can-annular combustion system was selected instead of the silo combustor commonly used in E-class turbines. Due to its larger size, the silo combustor requires a greater amount of cooling air and material consumption, resulting in increased maintenance and repair costs. Furthermore, its application is not suitable for F-class turbines operating at higher pressure ratios and combustor temperatures. Therefore, the can-annular configuration was selected for the MGT-75 to improve efficiency, increase power output, and enhance maintainability.

A structured combustor development program was carried out through conceptual, preliminary, and detailed design phases. Initially, the main combustor dimensions were defined using a 0D design approach based on experimental correlations. Preliminary can combustor concepts were then developed using 3D-CAD modeling, followed by a reverse-flow burner design based on CFD and FEM analyses. The final detailed design included the combustor and its associated components.

The MGT-75 combustion system consists of 16 circumferentially arranged burners, combustor liners, and transition pieces integrated within the turbine casing. Compressor discharge air is distributed between combustion, dilution, and cooling functions, while extracted cooling air is supplied to turbine hot-section components. Each combustor can is equipped with a high-energy igniter, a flame detector, and instrumentation systems for monitoring and protection. Flashback detection is performed using burner thermocouples, and dynamic pressure sensors are used to detect combustion instabilities. Maintenance and inspection are also facilitated through casing manholes.

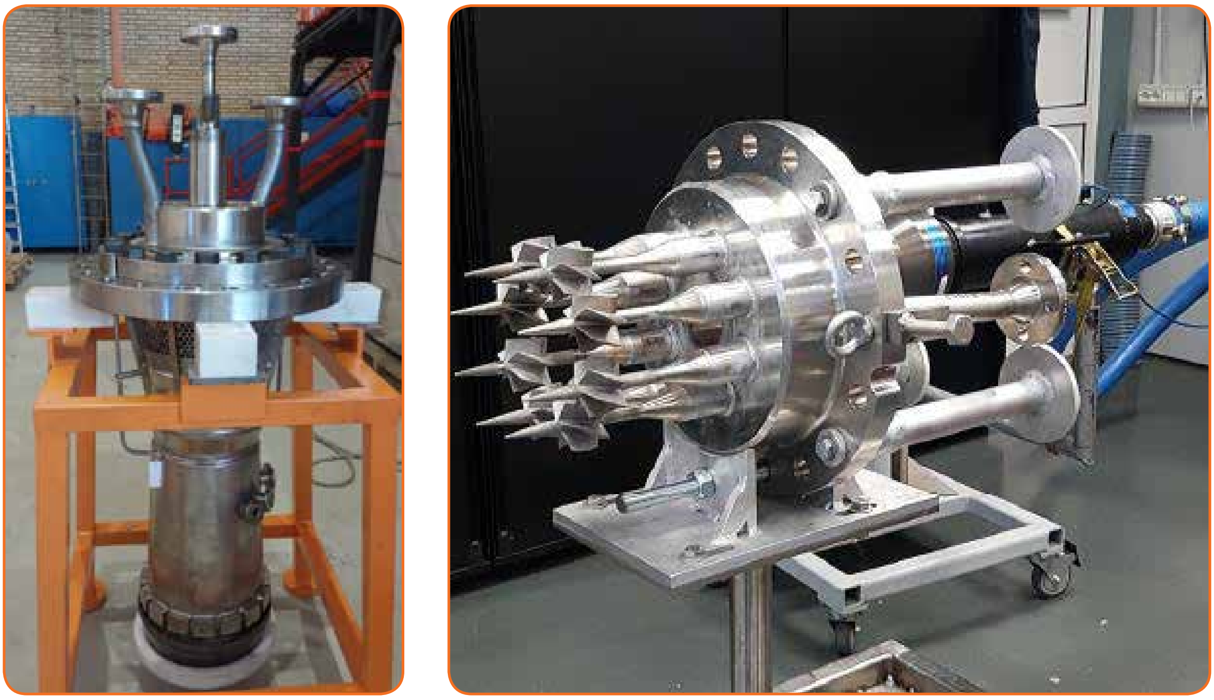

Figure 8- One of the MGT-75 Combustor Cans

Following the detailed design, thermo-mechanical assessments were performed to verify the structural integrity and durability of critical combustor components. Thermal loads and stationary thermal stresses were evaluated under base-load conditions using Finite Element Analysis (FEA). The Neuber approach was applied to account for material plasticity, and the calculated stress and temperature values were compared with creep-life data of HS 188 material to estimate component lifetime.

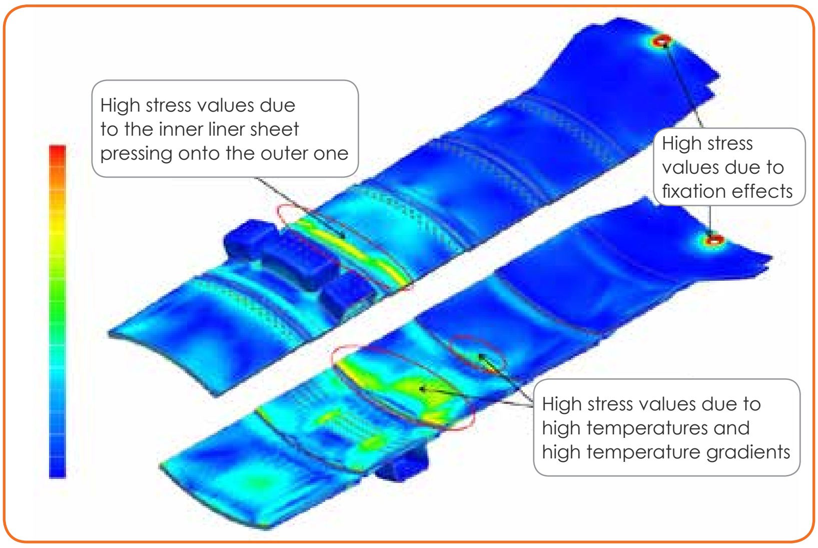

Figure 9- Stress Distribution of the MGT-75 Combustor Liner after Employment of the Neuber Procedure

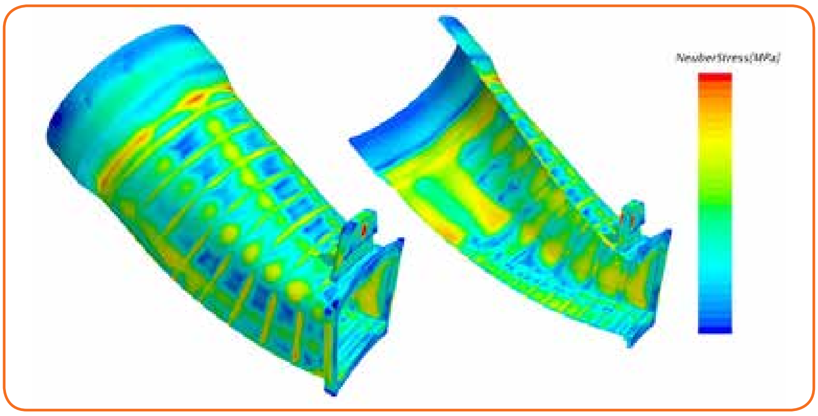

Figure 10- Stress Distribution of the MGT-75 Combustor Liner after Employment of the Neuber Procedure

Turbine Section

The turbine development process was carried out through three phases: conceptual, basic, and detailed design. In the conceptual phase, a one-dimensional aerodynamic design was performed based on cycle requirements and engine performance targets. The number of turbine stages, cooling air requirements, rotor configuration, and material selection were determined considering operating conditions.

During the basic design phase, the aerodynamic flow path and preliminary cooling system were developed using a vortex design approach. Blade loading, airfoil geometry, flow annulus, blade counts, and secondary air system parameters were defined. The aerodynamic design was iteratively optimized to improve turbine efficiency and power output while reducing rotor thrust, and preliminary stress analyses were performed to verify structural feasibility.

The detailed design phase included three-dimensional blade design, detailed cooling optimization, and secondary air system refinement. After final design review, the turbine configuration was established to meet the MGT-75 aerodynamic, thermal, and mechanical requirements. The hot gases expand through a four-stage axial turbine equipped with high-temperature superalloy blades and advanced cooling technologies, including film, vortex, and convection cooling. Thermal Barrier Coatings (TBCs) are applied to critical blade rows, with single-crystal and directionally solidified superalloy castings used for the first and second-stage blades, respectively.

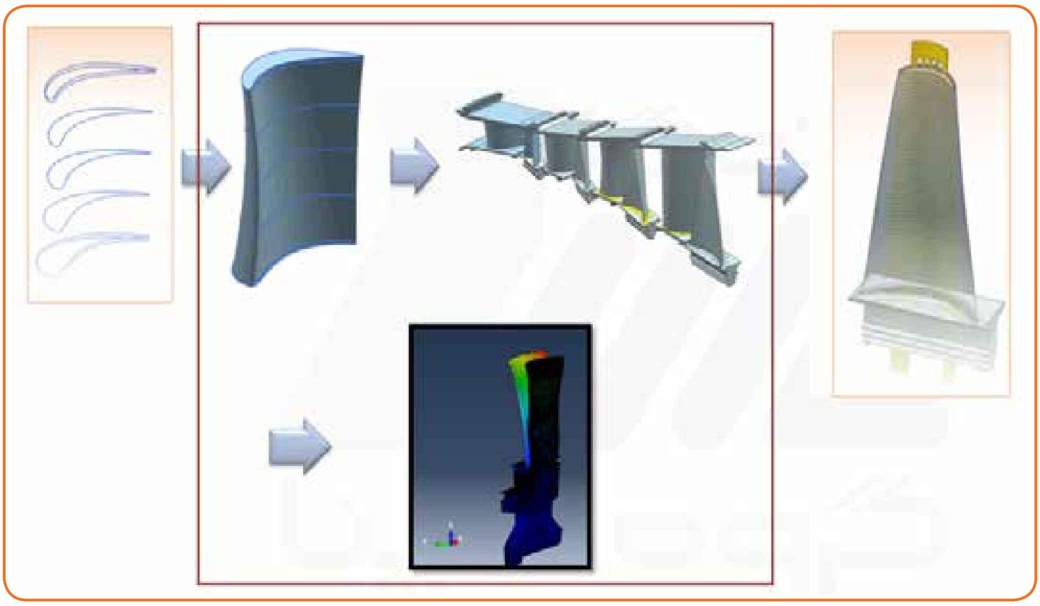

Figure 11- Flowchart of the MGT-75 Blade Design Methodology

The cooling system maintains acceptable blade and rotor temperatures by supplying cooling air through internal passages and blade roots, reducing thermal stresses during load variations and rapid start-up conditions. The first two turbine stages use combined film and internal cooling, while the later stages rely on convection cooling.

The final turbine design was validated through thermo-mechanical analyses using FEA. Temperature and stress distributions confirmed the effectiveness of the cooling system and material selection. The calculated von Mises stresses in critical regions, including the blade root and trailing edge, remained below the yield strength of the selected superalloys, confirming the adequacy of the aerodynamic and structural design.

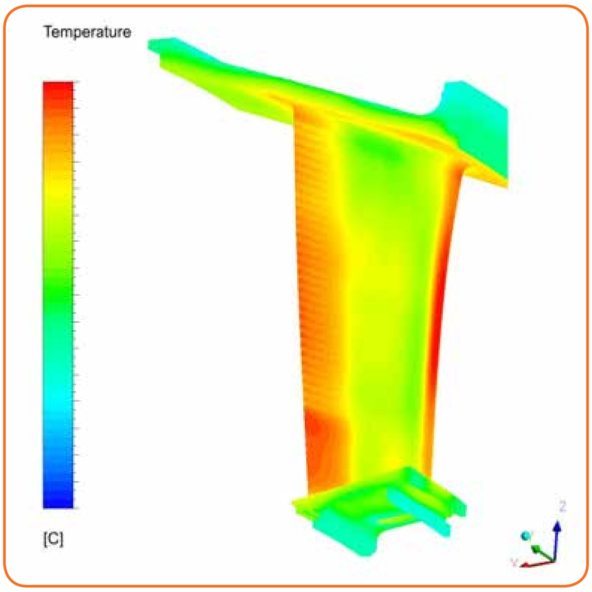

Figure 12- Temperature Distribution Contour across the Third-Stage Turbine Vane of the MGT-75

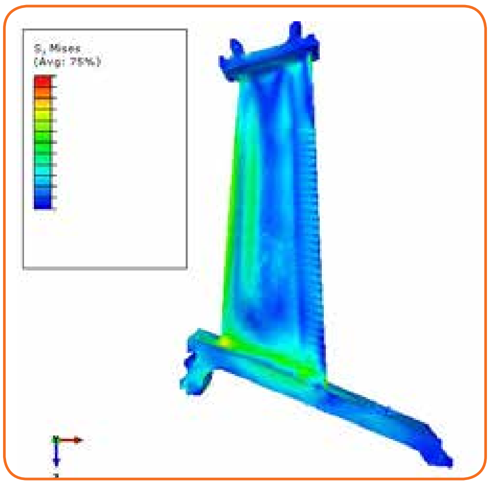

Figure 13- Von Mises Stress Distribution Contour for the Third-Stage Turbine Vane of MGT-75

Rotor

The rotor integrates the compressor and turbine sections into a single shaft supported by bearings at both ends. It consists of a front hollow shaft, fifteen compressor blade disks, a center hollow shaft, four turbine blade disks, and a rear hollow shaft. These components are held together by a single central tie bolt with a clamping nut located at the turbine end. In addition, the rotor includes four balancing planes for low-speed and high-speed balancing, and four additional planes designed for field balancing.

Each rotor disk incorporates radial Hirth serrations on both sides. These serrations provide precise radial alignment between the rotor sections, ensuring torque transmission and allowing free relative radial expansion and contraction. The construction results in a lightweight, high-stiffness, self-supporting drum structure. Consequently, the rotor can be supported by only two bearings located at the front and rear shaft sections. The bearing at the compressor end is a combined journal and thrust bearing designed to accommodate the axial rotor thrust.

The cooling air passes through the rotor via two independent circuits separated by an internal drum structure. This cooling configuration ensures that the rotor drum and the turbine section are entirely enveloped by the cooling medium. Consequently, additional thermal stresses that could induce rotor distortion during load transients and start-up cycles are mitigated. The adopted cooling air routing also imposed specific constraints on the rotor support and damping arrangement.

In the MGT-75 gas turbine rotor, conventional damping systems commonly employed in E-class turbine rotors were not feasible due to the configuration of the cooling air flow path, which would be obstructed by these systems. Therefore, element dampers are used in the design of the MGT-75 rotor.

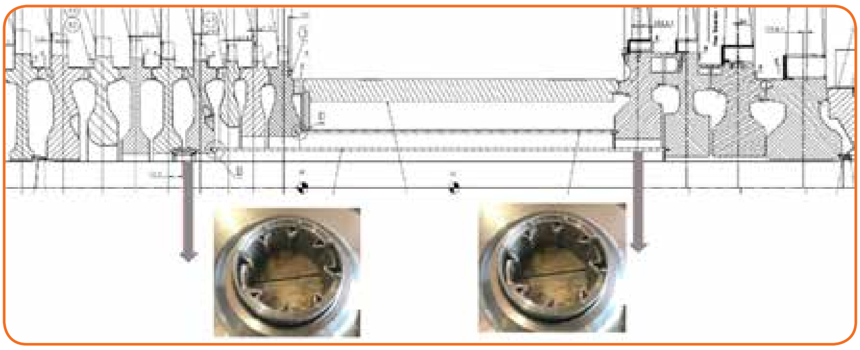

Figure 14- MGT-75 Gas Turbine Rotor and Its Damping Elements

A comprehensive rotor-dynamic assessment was subsequently performed to verify the dynamic behavior and mechanical integrity of the proposed rotor configuration. The rotor and bearings were modeled using the DyroBes software according to API 684. Four design criteria were evaluated to ensure a successful design. These criteria are as follows:

- The natural frequencies must be sufficiently separated from the specified operating ranges.
- The critical speeds associated with the bending modes must be sufficiently separated from the specified operating ranges.
- In the unbalance response analysis, the shaft and bearing vibration levels must remain below the specified limits.
- The strength and fatigue criteria must be satisfied under bending stresses caused by electrical faults.

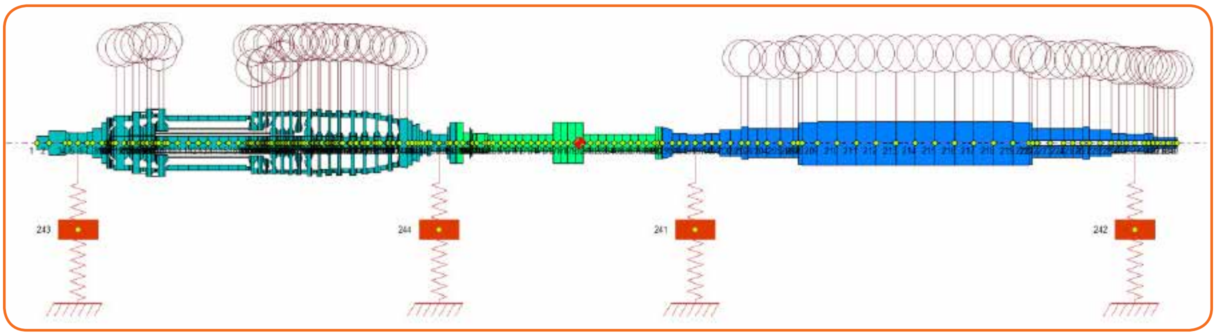

Figure 15- Reduced-Order Model of the MGT-75 Gas Turbine Shaft Train

Figures 16 and 17 show the calculated first torsional mode shape and shear stress due to the out-of-phase synchronization fault in the compressor journal, respectively.

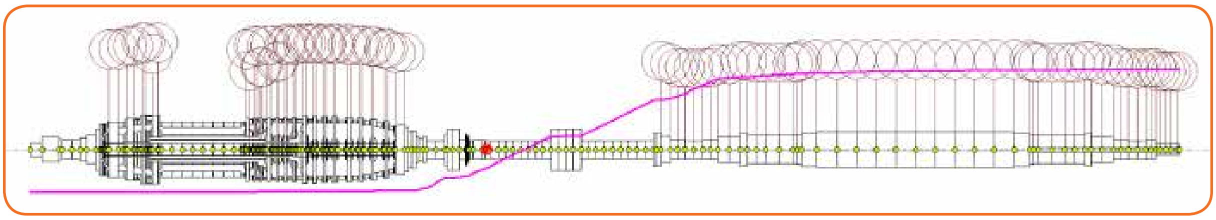

Figure 16- MGT-75 Rotor Train First Torsional Mode Shape

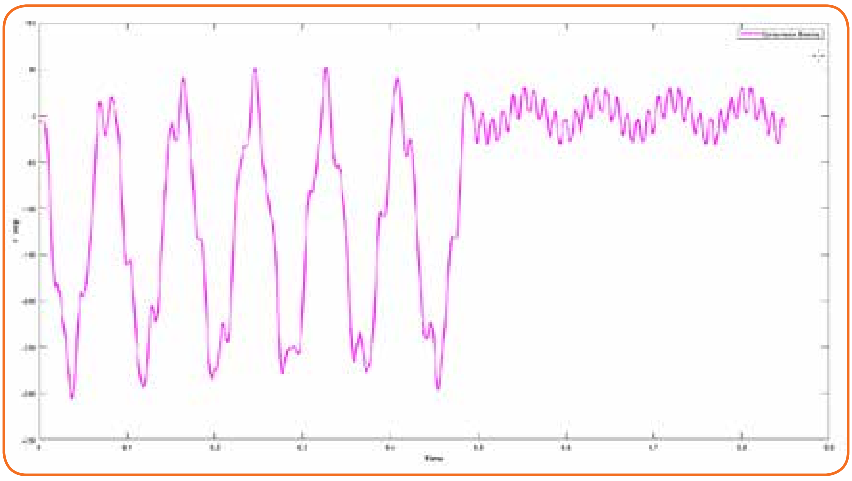

Figure 17- Shear Stress due to the Out-of-Phase Synchronization Fault in the Compressor Journal

The rotor dynamic assessment confirmed that all critical speed, vibration, and strength requirements specified by the design criteria were successfully met, demonstrating the mechanical robustness of the rotor system.

Casing

The casing structure of the MGT-75 gas turbine was designed to enable manufacturing by welding. An axial split flange divides the casing into two sections, while a horizontal split flange separates it into an upper and a lower part. A steady-state FEA calculation was performed under base-load conditions to design and evaluate the adequacy of the bolted connections, which were designed in accordance with VDI 2230.

Special attention was devoted to the design and verification of the flange and bolted joint system, as these interfaces govern both structural integrity and casing leak tightness. In the structural assessment of the bolted connections, casing leak tightness was evaluated by requiring the contact pressure to remain above 3.6 N/mm² throughout the sealing interface. This threshold corresponds to twice the maximum internal pressure of 18 bar (1.8 N/mm²), providing a safety factor of 2. The contact pressure across all contact faces was examined to evaluate the adequacy of the flange connections, with particular attention paid to the interfaces between different casing segments. Figure 18 illustrates the contact pressure distribution at various flange locations. The areas where the contact pressure falls below the specified limit are shown in grey.

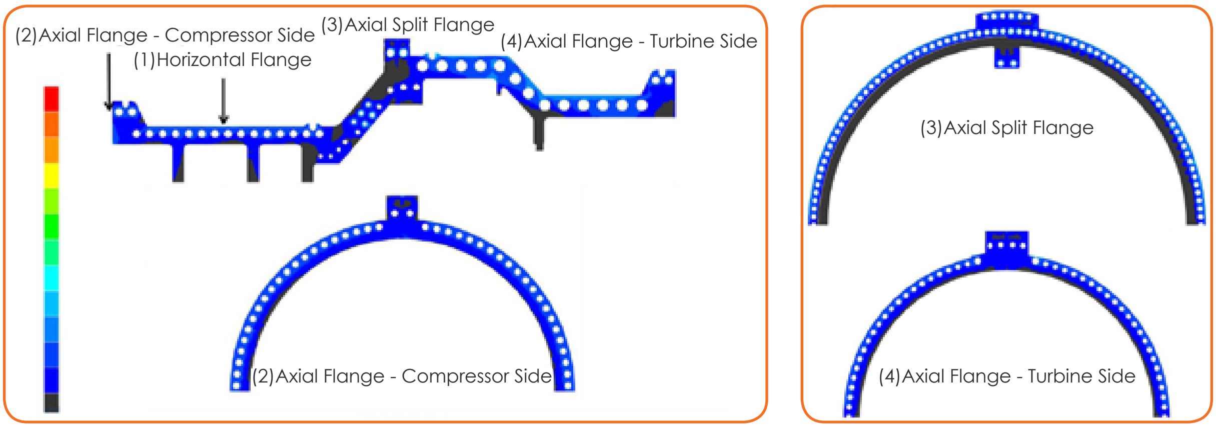

Figure 18- Contact Pressure Distribution of the Casing at Different Flange Locations

In addition to the steady-state assessment of the bolted joints, the thermo-mechanical behavior of the casing was also investigated under transient operating conditions. The transient behavior of the MGT-75 casing structure was evaluated in two phases. In phase 1, a transient thermal simulation was performed to calculate the thermal behavior during the start-up process. In phase 2, the time-dependent temperature information obtained from phase 1 was used as the input for a transient linear elastic FEA, which allowed quantification of the transient thermal stresses and deformations. The analyses described above were performed on the complete casing system, whose overall architecture is summarized below.

The pressure-retaining outer casing, which is common to the compressor, combustion, and turbine sections, consists of five parts:

- Compressor inlet casing containing the compressor bearing housing
- Compressor stator blade carrier I
- Combustor casing containing compressor stator blade carriers II, III, and IV, and the combustor cans

- Turbine casing containing turbine blade carrier and transition pieces
- Exhaust casing containing the turbine bearing housing

All casing parts are horizontally split, allowing for easy maintenance. All upper parts of the carriers and casings can be opened separately, providing access to the interior of the turbine. The compressor and turbine vanes are inserted into vane carriers; the turbine vane carriers can be removed and installed without removing the rotor. After removing the upper half, the lower vane carrier sections can be rotated 180° using the rotor as a rollout device and then lifted off.

Concluding Remarks

The present work described the design and development of the MGT-75 gas turbine, an advanced F-class heavy-duty machine intended to achieve high efficiency, low emissions, operational flexibility, and reliable performance for modern power generation applications. To better illustrate the technological position of the MGT-75 gas turbine, its main specifications are compared with those of the latest version of MAPNA E-class gas turbine (MAP2C). The comparison is presented in Table 2.

Table 2: Comparison of Main Specifications of the MGT-75 and MAP2C

	Parameter	MGT-75	MAP2C
1	GT Power at Generator (MW)	222	190
2	GT Efficiency (%)	39.1	36.5
3	Turbine Inlet Temperature (°C)	1220	1090
4	Compressor Pressure Ratio	18:1	12:1
5	Exhaust Mass Flow Rate (kg/s)	559	555
6	Turbine Exhaust Temperature (°C)	571	542
7	Operating Frequency (Hz)	50	50

As shown in Table 2, the MGT-75 achieves higher power output, efficiency, turbine inlet temperature, and compressor pressure ratio compared with the MAP2C gas turbine, reflecting the technological advancements incorporated into the new design.

The final design combined advanced compressor aerodynamics, a dry low-NOx can-annular combustion system, modern turbine cooling technologies, and a high-stiffness rotor structure to achieve competitive performance in both simple-cycle and combined-cycle operation. Furthermore, the horizontally split casing configuration and modular arrangement of major components improved accessibility and simplified maintenance procedures. Comprehensive CFD, rotor-dynamic, thermal, and structural analyses confirmed that all major subsystems satisfied their respective aerodynamic, mechanical, and durability requirements under both steady-state and transient operating conditions. Overall, the successful completion of the MGT-75 development program demonstrated MAPNA's capability in the design and integration of advanced F-Class gas turbine technologies and established a robust platform for future performance improvements and product evolution.

2

From Design to Testing: TUGA's First High-Pressure Gas Storage Compressor Unit

Moradi, Saeed
Javadi, MohammadAmin
Pourtaba, Hamidreza
Ghobadi, Mohsen

MAPNA Turbine Engineering & Manufacturing Co. (TUGA)

Introduction

Effective energy management and a reliable gas supply have been among the fundamental challenges facing Iran in recent years. One approach to addressing these challenges is the storage of natural gas during periods of low demand and its withdrawal during periods of peak consumption. Underground gas storage requires compressors capable of delivering gas at high pressures and flow rates to facilitate gas injection.

In this regard, the project for the design and manufacturing of high-pressure gas storage compressors was carried out at TUGA. Further details on the design of these compressors are provided in the third article of Technical Review No. 21. This turbo compressor package comprises two centrifugal compressors: a Low-Pressure (LP) compressor and a High-Pressure (HP) compressor, arranged in straight-through and back-to-back configurations, respectively, and increases the gas pressure from 49 bar at the Iran Gas Trunk-line (IGAT) to 345 bar at the compressor outlet.

Following the design, manufacturing, and assembly of these compressors at TUGA, they successfully completed all specified tests according to the client's material requisitions and related international standards and codes, before being delivered to the client. The tests discussed in this article include hydrostatic test of pressured parts, high-speed rotor balancing, mechanical run test, performance test, and assembled compressor gas leakage test.

Hydrostatic Test of Pressured Parts

In accordance with the requirements set forth in API 617, to verify the strength and leak tightness of the compressor pressure-containing parts, including the casing and end covers, these components of the LP and HP compressors were subjected to a hydrostatic pressure test using the existing test bench. The test pressure was 276 bar for the LP compressor components and 588 bar for the HP compressor components. The specified test pressure was maintained for 30 minutes for all components. After successfully passing the hydrostatic pressure test, the components proceeded to the subsequent manufacturing operations.

Figure 1- Hydrostatic Pressure Test of Casing

High-speed Rotor Balancing

High-speed balancing of the assembled rotor is a critical step in the rotor manufacturing process. The quality of rotor balancing has a significant impact on vibration levels, compressor reliability, and service life. This is particularly important for the LP and HP compressor rotors of the gas storage field, which operate at a Maximum Continuous Speed (MCS) of 13,380 rpm. The balancing test was successfully completed, with vibration levels below 1 mm/s for the bearings on both ends of the LP and HP rotors.

Figure 2- High-Speed Balance of LP Rotor

Mechanical Run Test

Another mandatory test specified by API 617 for centrifugal compressors is the Mechanical Run Test. In this test, the assembled compressor is driven at various speeds by a test driver, and parameters including vibration levels, bearing temperatures, and oil inlet and outlet pressures are measured. The LP and HP compressors of the case-study unit were individually subjected to the mechanical test using the TUGA's compressor test bench. During the tests, all measured parameters remained within the permissible limits; therefore, both compressors passed the Mechanical Run Test successfully and then proceeded to the next stage of testing.

Figure 3- Mechanical Run Test of the LP and HP Compressors

Performance Test

The performance test was conducted to precisely evaluate the aerodynamic characteristics of the compressors under specified operating conditions. In accordance with API 617, the test methodology specified in ASME PTC 10 was applied to validate the compressor performance against the guaranteed performance curves.

During the test, the aerodynamic behavior of the machines was assessed at a minimum of five operating points, covering the entire operating range, including boundary regions such as surge and overload limits. Key parameters, including pressure, temperature, and mass flow rate, were monitored throughout the process. The testing was performed using air as the test fluid at the specialized TUGA compressor test facility.

The subsequent data analysis and the corresponding performance curves, specifically pressure ratio versus flow rate and efficiency versus flow rate, demonstrated full compliance of both LP and HP compressors with the design performance maps and guaranteed performance curves. Therefore, the results confirmed that both compressors met the specified aerodynamic performance requirements over the tested operating conditions.

Figure 4- Performance Test of HP Compressor

Assembled Compressor Gas Leakage Test

The assembled centrifugal compressors underwent a gas leakage test to verify the gas-tightness of the compressor casing and its joint connections. The gas leakage test for the gas storage compressors was conducted at the TUGA air test facility following completion of the Mechanical Run Test. The compressors were mounted on the test stand using suitable structural supports. All process gas connection branches on the compressor casing were fitted with blind flanges during the test. All contract-specified internal components of the compressor, including the bearings and shaft seals, were installed in their normal operating configuration during the test.

This test sequence included pressurization, maintaining the pressure, recording the required measurements and soap-bubble testing. In this process, the test pressure was 79 bar for the LP compressor and 179 bar for the HP compressor, and the pressure was maintained for 30 minutes. Both compressors met the predefined acceptance criteria, and the test results complied with the specified test requirements.

Figure 5- Gas Leakage Test of LP and HP Compressors

Concluding Remarks

Based on the test results and successful completion of all required tests, the first high-pressure gas storage compressor unit comprising the gearbox, LP and HP compressors was delivered to the project client after being packaged at TUGA. The satisfactory completion of the testing program confirmed the mechanical integrity, aerodynamic performance, and gas-tightness of the compressors, as well as their compliance with the specified requirements. The implementation of this project also demonstrated TUGA's capability in the design, manufacturing, assembly, and testing of large-scale centrifugal compressors for critical gas-storage applications. Developing such capabilities can contribute to efficient resource management and energy security in Iran.

Figure 6- The First High-Pressure Gas Storage Compressor Unit after Packaging in TUGA

3

MGT-30 On-Site Test Using Automated Data Processing

Ghalandari, Parvin
Azizi, Rohollah

MAPNA Turbine Engineering & Manufacturing Co. (TUGA)

Introduction

The MGT-30 gas turbine is widely utilized in mechanical-drive and power-generation applications. During manufacturing, the turbine undergoes a series of mechanical and performance tests on a factory test stand, conducted in accordance with standard procedures to verify that all guaranteed parameters are achieved. However, in some cases, factory test data may be unavailable, incomplete, or unusable, making on-site performance testing essential for confirming compliance with performance guarantees under actual operating conditions.

On-site testing of mechanical-drive turbines presents unique complexities. Direct shaft-power measurement is unavailable and field measurements are often performed under conditions that are not optimized for testing. These issues make direct performance calculation difficult without a structured methodology.

To address these challenges, a systematic and automated framework has been developed for the MGT-30 as part of MapCycle, TUGA's integrated performance platform. In this framework, automated Exploratory Data Analysis (EDA) is used for data filtering and preprocessing, compressor gas power is determined using gas-property calculations based on ISO 20765, and a Python-based computational tool is used to calculate performance and generate standardized reports. This integrated approach enables accurate and repeatable on-site performance evaluation under real operating conditions.

This article describes the technical challenges associated with field testing of a gas turbine driven compressor and presents the developed methodology as a reliable, repeatable, and efficient alternative to factory testing, when factory test data are limited or unavailable.

Challenges and Approach for On-Site Power Determination

In on-site configurations, direct shaft-power measurement is unavailable because the turbine drives the gas compressor through a rigid coupling and no torque-sensing instrumentation exists in the train. Consequently, calculated compressor gas power, derived from measured process conditions, becomes the primary indicator of gas turbine performance and is essential for acceptance testing, troubleshooting, and long-term performance evaluation.

Accurate determination of gas power requires both reliable thermodynamic properties and high-quality site data. This task is complicated by variations in natural gas composition, which modify density, compressibility, and enthalpy, as well as by the presence of noise, outliers, and timing inconsistencies in field measurements. Without systematic preprocessing and a robust thermodynamic framework, these factors can introduce significant errors into the final power calculation.

To ensure accuracy and traceability, the methodology adopts ISO 20765, the global standard for calculating thermodynamic properties of natural gas mixtures. The standard defines a reference-quality equation of state that allows consistent calculation of caloric and volumetric properties over a wide operating range. It specifies how gas composition should be defined and normalized, outlines procedures for computing real-gas behavior such as enthalpy, density, compressibility, and heat capacities, and includes consistency requirements that help verify alignment between calculated properties and measured field conditions.

Gas composition is obtained from accredited laboratory analysis, while suction and discharge pressures and temperatures are measured at the compressor. Because mass flow rate typically contributes the largest share of overall uncertainty, a venturi-type flowmeter installed at the compressor inlet is used for flow measurement, with its discharge coefficient validated during the surge test.

By combining high-quality site measurements with standardized thermodynamic procedures, the calculated gas power closely represents the actual work performed on the process gas and provides a reliable basis for evaluating gas turbine performance under real operating conditions.

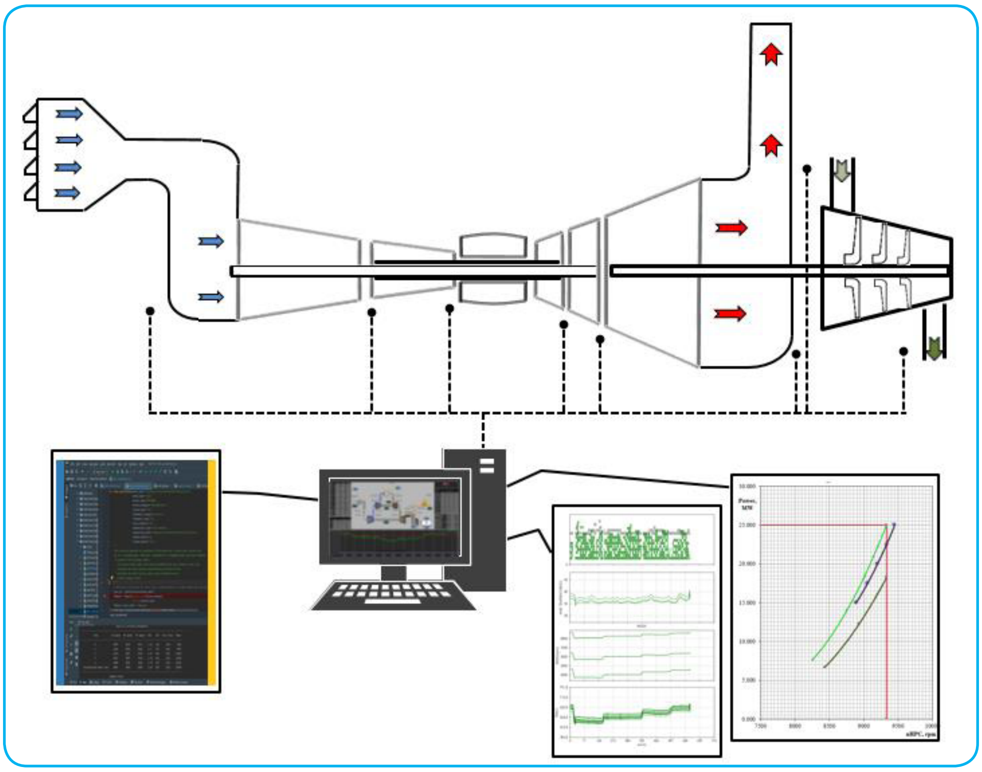

Figure 1- Turbo Compressor On-Site Test Schematic

On-Site Testing

On-site performance testing of turbo compressor units in a gas pipeline station differs significantly from controlled factory tests. The turbine operates as part of the integrated pipeline system, where its load is determined by compressor demand rather than the turbine's maximum capacity. As a result, test conditions are constrained by actual operating requirements, with limited flexibility to adjust flow or load.

The primary objective of the site test is to verify the performance and coordination of the turbine-compressor train under real conditions. For the turbine, this includes confirming operational limits such as shaft speed and gas generator exit temperature, while for the compressor, the test ensures stable operation across its map and alignment with design requirements. The test also validates control logic, limit protections, and driver-driven coordination across the permissible load range.

In stations with multiple parallel trains, load sharing is normally automatic to balance the total pipeline demand. During testing, manual adjustments may temporarily increase the load on the tested train within safe limits. This involves slightly reducing the load on other trains, adjusting turbine speed or control bias, and monitoring anti-surge valves to maintain compressor stability and overall pipeline balance. These adjustments allow the test train to reach nominal operating points even if the station is below full capacity.

A structured execution strategy is essential for reliable results. Coordination between operators and control engineers defines safe load adjustments and surge margins. During testing, load-sharing set-points are progressively modified while closely monitoring turbine constraints, compressor stability, and anti-surge valve behavior. Key process variables are recorded to create a consistent dataset that supports gas power calculations and subsequent performance evaluation.

Programming and Data Processing

Traditionally, data preparation and analysis for turbo compressor site tests were performed manually or with partially automated scripts, which were time-consuming, error-prone, and difficult to reproduce. To overcome these limitations, a fully automated Python-based framework has been developed, implementing an in-house EDA methodology that transforms raw sensor data into validated performance results. This framework provides a reproducible, auditable, and scalable solution, capable of handling all aspects of site-test data processing from preprocessing to final calculation.

Python was selected for this framework due to its extensive scientific ecosystem, including libraries for data handling, numerical computation, visualization, thermophysical property integration, and automated reporting. The framework integrates these capabilities into a single, consistent system that ensures traceability and quality at every stage of the analysis.

EDA forms the foundation of the framework. Raw field data often contain noise, misalignment, missing values, or outliers resulting from sensor drift, communication interruptions, or transient process conditions. The framework systematically addresses these challenges by examining the data, producing statistical summaries and visualizations, and performing sensor health diagnostics to ensure that only reliable, consistent data are used for performance calculations.

Processing begins with metadata removal, isolating non-numerical headers or operator notes for documentation while extracting structured measurement data. Sensor tags are standardized through a configurable mapping system, harmonizing plant-specific naming conventions and enabling consistent datasets across the process. Summary statistics and visualizations help detect anomalies, verify thermodynamic consistency, and provide an intuitive understanding of system behavior.

Data from multiple acquisition systems are synchronized to a common time base, correcting irregular sampling intervals, missing timestamps, and clock offsets. Systematic data cleaning addresses missing values, transient spikes, noise, and physically implausible readings while preserving genuine operational behavior. Sensor health evaluation ensures that all channels are accurate, consistent, and trustworthy before analysis.

A critical feature of the framework is automated steady-state detection. Site-test data often include transients due to load changes, control adjustments, or measurement fluctuations. The framework applies a rolling window technique to identify intervals where key parameters, such as ambient temperature, turbine speed, and exit temperature, remain stable. Statistical measures including mean, standard deviation, and coefficient of variation are evaluated within each window against predefined thresholds to classify steady and transient periods. By focusing on representative operating conditions, this method ensures that only equilibrium data are used for ISO 20765-based gas power calculations and performance evaluation.

Through this integrated approach, the Python-based framework provides a robust, automated, and reproducible solution for site-test data processing, enabling accurate and traceable assessment of turbo compressor performance under real operating conditions.

Analysis Phase within the Automated Framework

Once preprocessing, cleaning, and steady-state detection are complete, the refined dataset enters the analysis phase. At this stage, the framework transforms validated site measurements into actionable performance indicators for the gas turbine.

The first step in analysis is the calculation of compressor gas power, representing the mechanical energy absorbed by the compressor and, equivalently, the power delivered by the turbine shaft under steady-state conditions. The framework ensures that only steady intervals, identified in the preprocessing stage, are used in these calculations, guaranteeing representative results. Building on the calculated gas power, the turbine's behavior is evaluated using similarity corrections. Measured turbine parameters, typically collected at multiple intermediate load points during the site test, are corrected to the reference condition. The analysis further identifies limiting parameters, such as maximum spool speed or gas generator exhaust temperature, which define the turbine's base-load constraints.

Throughout the analysis, the framework automatically generates visualizations and reports. Plots of key process variables and turbine performance curves are produced. Both Word and Excel reports include all calculations, intermediate results, graphical illustrations, and descriptive notes, providing a complete and traceable record of the site-test performance evaluation.

Field Application: Non-OEM Gas Turbine Site Test Using the Developed Framework

The developed framework, originally implemented for MGT-30 gas turbine testing, was successfully applied to a non-OEM three-spool gas turbine. At the Gachsaran station, TUGA commissioned the ZORYA DG90 turbine and, having no prior experience testing this model, performed an on-site performance evaluation using the developed automated framework, which handled all stages of data preparation, including reformatting, synchronization, cleaning, and steady-state detection.

Once steady operating regions were identified, compressor gas power was calculated, followed by turbine performance analysis using similarity corrections. The results successfully generated turbine characteristic curves, showing relationships between power, speed, and gas generator exit temperature. Operational limits, such as maximum generator speed and exit temperature constraints, were identified, defining the base-load parameters for the tested configuration.

This experience demonstrated that the framework can handle other turbine models, data structures, and sensor naming conventions, while automatically generating accurate and reliable results. The experience confirmed that the methodology is suitable for both OEM and non-OEM turbines operating under real site conditions.

Concluding Remarks

The developed Python-based framework provides a fully automated workflow for on-site performance evaluation of mechanical-drive gas turbines, covering the entire process from raw data acquisition to final report generation. By integrating automated data preprocessing and steady-state detection through custom-developed EDA, compressor gas-power determination, turbine similarity corrections, and standardized reporting, the framework produces validated, traceable, and thermodynamically consistent performance results with minimal manual data handling.

The proposed methodology enables reliable performance assessment under real operating conditions, where measurement constraints and environmental variations often limit the applicability of traditional testing approaches. Automated data filtering and consistency checks significantly reduce uncertainties associated with manual data handling, while the structured computational workflow improves repeatability of the evaluation process.

Furthermore, the framework is scalable and adaptable to different operating scenarios and compressor configurations, making it suitable not only for performance verification when factory test data are unavailable, but also for routine operational monitoring and performance trending throughout the turbine lifecycle. By bridging the gap between controlled factory testing and real-field operating environments, this approach offers a practical and efficient alternative to conventional factory testing, enabling accurate performance verification directly at the operating site.

4

CFD-Based Methodology for Axial Thrust Prediction in Heavy-Duty Gas Turbines

Mehrabi, Ali
Mirnia, Mohammad
Ranjbaran, Alireza

MAPNA Turbine Engineering & Manufacturing Co. (TUGA)

Introduction

In parallel with main modules of design and thermal performance evaluation of gas turbine, accurate prediction of rotor axial thrust is a critical aspect of the design phase with regard to safe machine operation. Axial forces acting on the rotor directly affect the selection, sizing, and lifetime of thrust bearings, as well as the structural integrity and dynamic behavior of rotating components. In fact, inaccurate estimation of these forces may lead to excessive bearing loads resulting in undesirable mechanical failures. Therefore, reliable thrust calculation methodologies are essential throughout the design and validation stages of new or upgraded gas turbines to ensure mechanical integrity, optimal bearing design, and overall system reliability, particularly under complex aerodynamic and thermal operating conditions.

Early analytical models for thrust prediction relied on simplified one-dimensional flow theories, estimating thrust by balancing of axial forces in which experimental correction factors, obtained from gas turbine field tests, were essential to achieve acceptable results. However, with development of digital computation, more advanced numerical techniques have become available now, enabling more accurate estimation of rotor thrust across various engine operating conditions.

In this article, a new methodology for calculating rotor thrust forces in the MGT-70 heavy-duty gas turbine, has been presented. The study integrates results from high-fidelity aerodynamic simulations of both compressor and turbine sections, three-dimensional CFD simulations of the Secondary-Air-System (SAS) paths under full-load and part-load conditions, and estimates pressure levels in turbine cavity spaces and rotating passages of the secondary air system based on centrifugal forces. Therefore, three-dimensional phenomena, including vortices, centrifugal forces, and pressure losses, have been taken into account, leading to highly accurate results compared to simple one-dimensional models. To validate the computational results, load cells were installed on the turbine bearing pads to provide experimental data for comparison between experimental measurements and numerical calculations.

MGT-70 Rotor Structure

The MGT-70 is a single-shaft, heavy-duty gas turbine with a sixteen-stage axial compressor and a four-stage turbine section mounted on a central rotor as shown in Figure 1. The rotor structure consists of compressor-side and turbine-side disks, all aligned by a central preloaded tie-rod. To ensure reliable torque transmission and secure mechanical integrity, Hirth-serrated couplings are employed between adjacent disks. A central hollow shaft spans the rotor intermediate space, serving both as a structural connection between the disks and as a passage for delivering cooling air extracted from the final compressor stages to the turbine blades. In addition, two shafts are installed at the front and rear ends of the machine, providing support for the main bearings.

Regarding air partitioning, the compressor rotor is divided into three blocks by damping rings positioned at the 6th, 9th, and 13th disk bores. This configuration enhances the rotor's overall stiffness, leading to reduced vibration amplitudes at higher critical speeds. All rotating compressor components are enclosed by air extracted from the main flow during operation. Within each rotor block, this air enters and exits the cavities through the Hirth serration gaps, generating a centrifugal-driven circulation that influences the thermal and pressure distribution across the disk bodies.

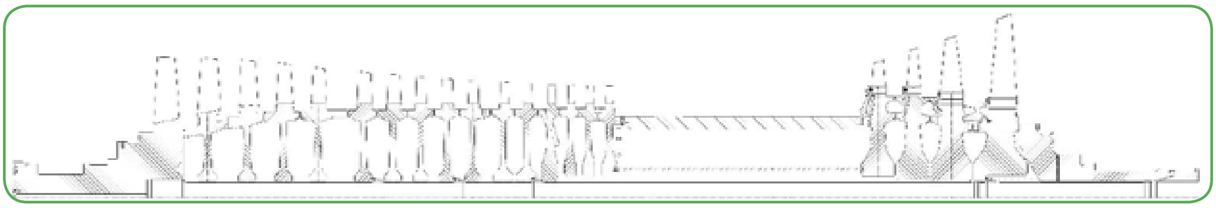

Figure 1- Schematic of MGT-70 Gas Turbine Rotor

A significant portion of the secondary airflow inside the rotor is directed toward the turbine blade cooling passages. This flow contributes to axial forces acting on both rotating and stationary components of the turbine section. Two turbine exhaust struts are designed as hollow passages to deliver lubrication oil to the rear bearing assembly. Also, air extracted from the outer region of the 5th stage is routed through a hollow strut and delivered to the cavity surrounding the rear hollow shaft, as shown in Figure 2. This configuration acts as the turbine thrust piston, which effectively generates a counteracting force to balance the net axial thrust imposed on the rotor. In addition to these secondary-air-induced forces, further axial loads arise from aerodynamic interactions between the main gas-path flow and the rotating blades in both the compressor and turbine sections. At the compressor side of the rotor, the front bearing housing contains both active and passive thrust pads. The active bearing resists the axial load directed toward the turbine exhaust during steady operation, while the passive bearing carries axial forces directed toward the compressor side, which may occur during transient conditions such as start-up.

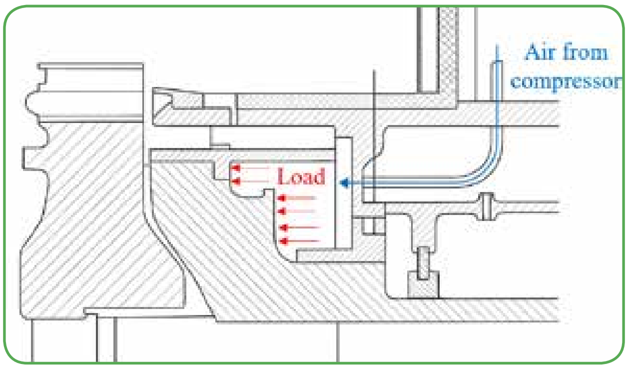

Figure 2- Thrust Piston Balance

Thrust Calculation Methodology

As mentioned previously, to evaluate rotor axial loads in gas turbine engines, different approaches can be employed, among which one-dimensional models are widely used as a preliminary and conventional assessment approach. The 1D methods import a simplified geometric description of rotor components together with pressure estimations obtained from compressor, turbine, and SAS calculations to compute the axial thrust contribution of each subsystem, ultimately yielding the net rotor thrust and the corresponding bearing loads. Generally, in one-dimensional methods, some calibration factors derived from experimental measurements are required to correct cavity pressures and ensure sufficient accuracy in total thrust predictions.

In a more precise hybrid approach, the one-dimensional framework for cavity modeling is retained, while three-dimensional CFD analysis is performed on the compressor and turbine flow-paths. By resolving the detailed aerodynamic loading on blades, endwalls, and shrouds, hybrid methods improve the accuracy of the flow path contribution to axial thrust. Nevertheless, the cavity pressures continue to be estimated through 1D formulation, which in turn necessitates the correction factors based on engine field test data. The flow diagram of the hybrid methodology is presented in Figure 3.

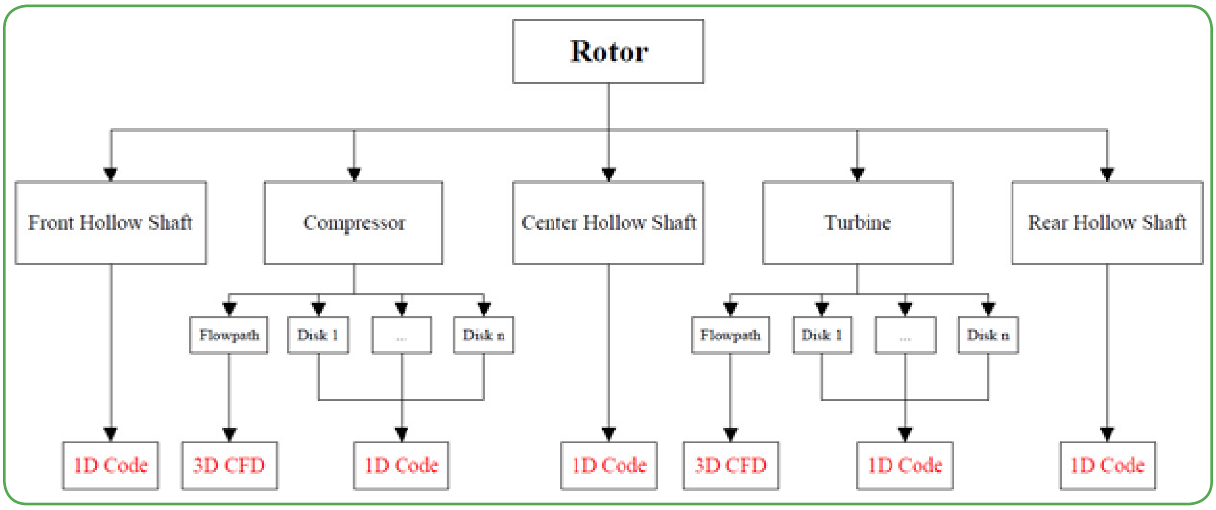

Figure 3- Flow Diagram for the Calculation of Rotor Thrust Using the Hybrid Method

Despite their applicability, the dependence of one-dimensional tools on estimated cavity pressures and calibration factors imposes inherent limitations on predictive capability. As noted above, 1D models require calibration coefficients obtained from experimental measurements to achieve acceptable accuracy. Consequently, each gas turbine must undergo dedicated test campaigns to generate the required validation data, which significantly increases the time, cost, and engineering effort associated with thrust-load prediction. Moreover, 1D methods are unable to deliver reliable thrust estimates for new designs or significantly modified engines, as no prior experimental data exist for calibration. This limitation is critical during the early design phase, particularly when selecting or sizing the thrust bearing. These constraints highlight the need for a more appropriate calculation approach capable of capturing three-dimensional flow structures and cavity interactions, thereby enabling accurate thrust evaluation in the absence of experimental data.

To overcome the inherent limitations of one-dimensional models and capture the detailed flow interactions within the rotor, a three-dimensional CFD-based methodology has been implemented. The rotor axial thrust calculation method, developed by TUGA, employs 3D CFD to evaluate the axial thrust generated by air or gas pressure acting on all rotating surfaces.

Accurate geometric data and CFD simulations of the gas turbine rotor components are required to determine the thrust force and consequently, the net loads acting on the bearings. As illustrated in Figure 4, the total axial thrust acting on a gas-turbine rotor originates from two primary sources: (1) flow path forces and (2) pressure forces. As mentioned above, the flow-path component consists of the axial momentum and pressure loads exerted on the blades, endwalls, and shrouds. The pressure-force component, however, arises from several distinct mechanisms within the rotor–stator cavity system. These include: (i) the axial loads acting on the blade roots, (ii) the thrust generated within the inter-disk cavities, both the upper and lower regions between adjacent rotor disks, and (iii) the axial forces associated with the air-transfer holes embedded in the rotor disks. Each of these pressure-induced loads is evaluated directly from the pressure field obtained through the three-dimensional CHT simulations. In most gas turbines, the flow path contributions to rotor thrust in the turbine and compressor sections are of comparable magnitudes, making accurate evaluation of cavity-induced forces particularly critical. Consequently, the three-dimensional approach employed in this study provides more precise and reliable calculations compared to conventional one-dimensional methods.

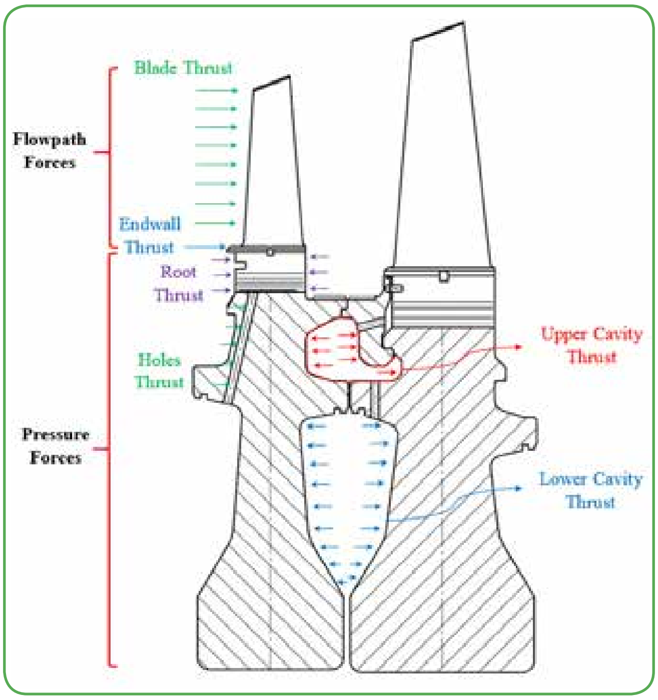

Figure 4- Types of Axial Forces

To enable three-dimensional simulations, the gas-turbine rotor must be partitioned into several sections. In the MGT-70 gas turbine, the rotor is divided into five main regions (the compressor, the turbine, the front hollow shaft, the center hollow shaft, and the rear hollow shaft) which form the basis of the solution methodology. Figure 5 illustrates the overall flow diagram used to compute the MGT-70 rotor axial thrust by decomposing the rotor into its major structural segments. A three-dimensional, multistage CFD aerodynamic simulation of the compressor and turbine, performed separately, provides the flow path force predictions. These simulations employ the k–ω SST turbulence model, widely recognized for turbomachinery applications, in combination with high-quality meshes across various operating conditions, including part and full-load cases. The air motion inside the three compressor blocks produces axial forces that contribute to the total rotor thrust. The thrust generated within these blocks is evaluated using the effective pressure acting on the cavity surfaces, induced by the centrifugal forces acting on the rotating air based on CFD simulations. In addition, due to the extraction of secondary air from the compressor stages, a full three-dimensional CHT analysis is performed in ANSYS CFX starting from compressor disks and extending through the turbine's rotating cavities.

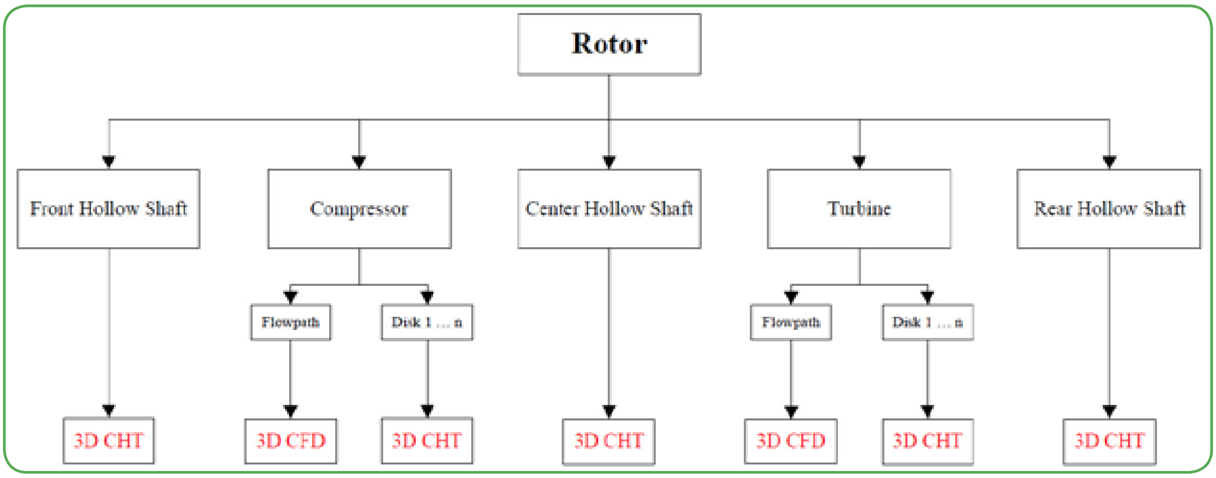

Figure 5- Flow Diagram for the Calculation of Thrust on the MGT-70 Rotor Using the 3D Method

To enable accurate representation of all rotor disks and the associated cavity flows, while simultaneously reducing the overall computational cost, a sector model is used, as illustrated in Figure 6, with the inlet and outlet boundary conditions appropriately adjusted to preserve the correct total mass flow rate. Two separate fluid domains are defined to properly capture the interaction of the secondary-air system with the rotating cavities. This CFD simulation provides the detailed pressure distribution required to quantify the axial thrust acting on the internal rotor components. Sufficient mesh resolution is applied to accurately resolve near-wall flow features and cavity interactions. An example of the mesh topology adopted in the current simulations is depicted in Figure 7. The static pressure distribution within the flow domains of the secondary-air system, turbine and compressor of the MGT-70 rotor is presented in Figures 8 to 10.

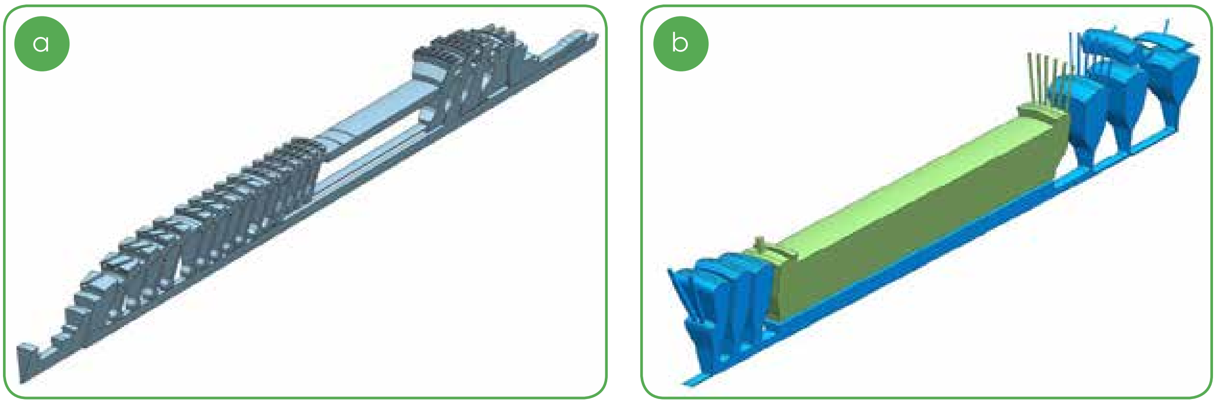

Figure 6- The Sector of MGT-70 Rotor Components (a) Solid Domain (b) Fluid Domain

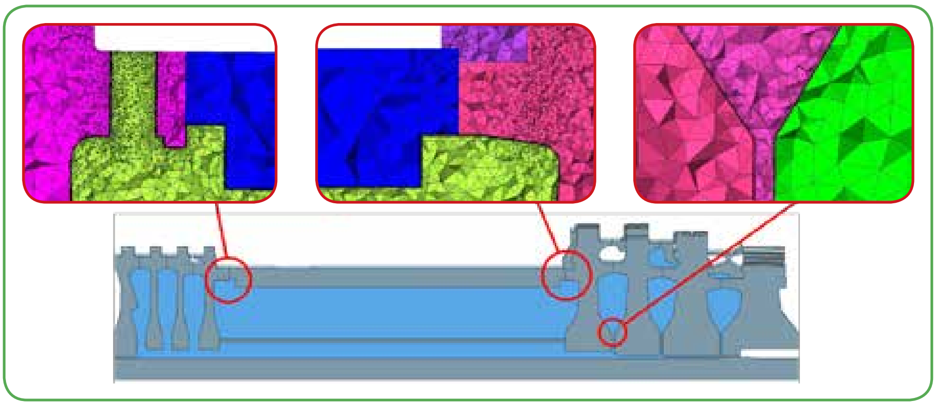

Figure 7- Mesh Topology Used for SAS Simulations of MGT-70 Rotor

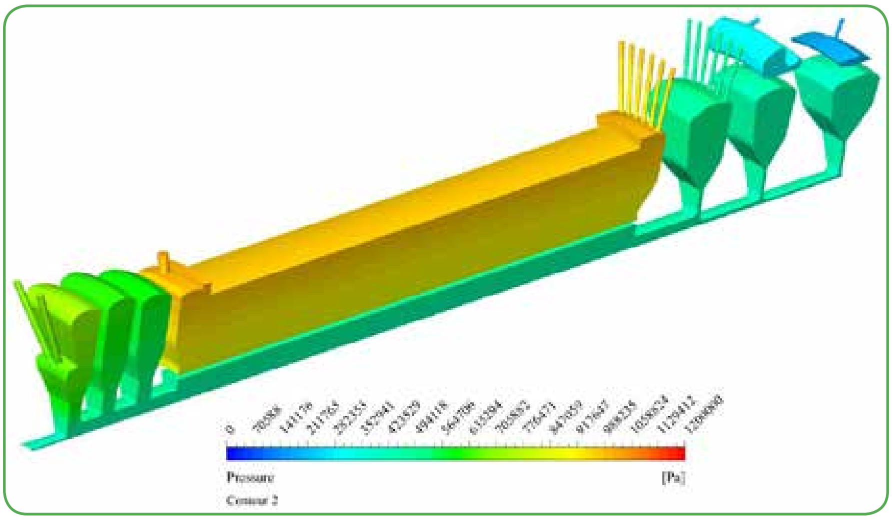

Figure 8- Pressure Distribution in SAS Domain

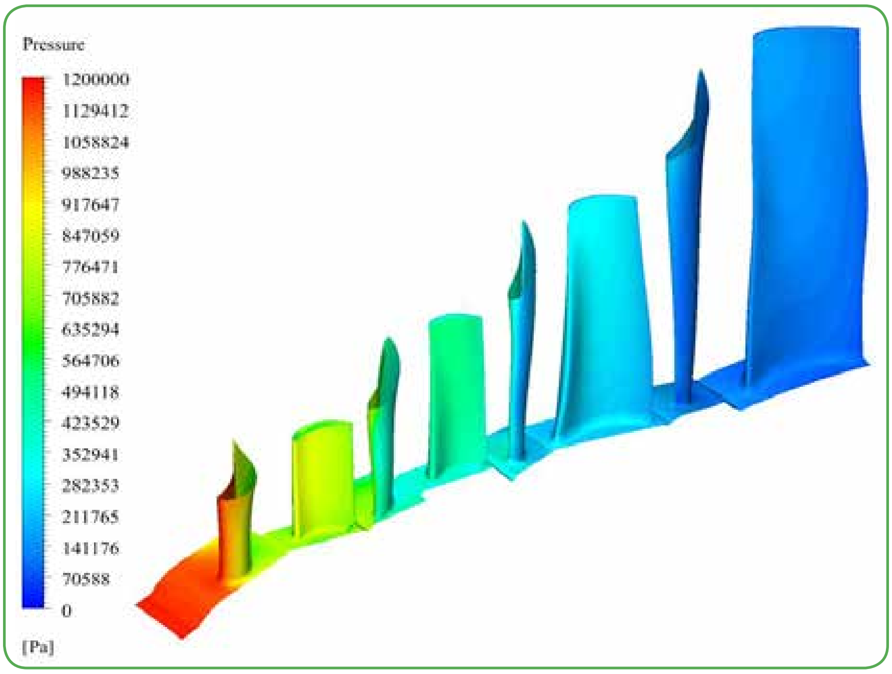

Figure 9- Pressure Distribution in Turbine Section

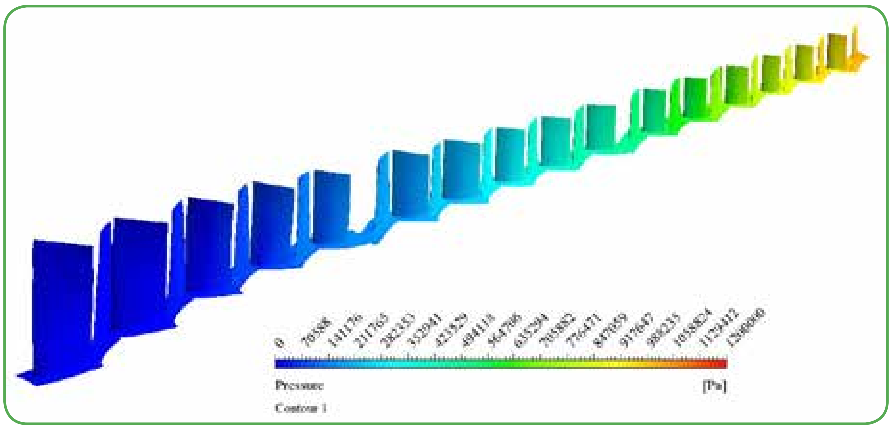

Figure 10- Pressure Distribution in Compressor Section

Figures 11 and 12 illustrate the axial thrust contributions acting on the MGT-70 gas turbine rotor in the base load condition. The results indicate that the turbine section flow path generates a dominant positive axial force, which is largely counterbalanced by the opposing thrust produced within the compressor section flow path. The comparable magnitude of these two forces confirms that flow path forces alone are insufficient to determine the net rotor thrust and that secondary pressure-driven components play an important role in the overall axial load balance. The hollow shafts and thrust piston introduce additional pressure forces that act in the opposite direction to the turbine-induced thrust, thereby mitigating the net positive axial load toward the turbine outlet. As shown in Figure 12, the thrust piston carries a considerable amount of negative axial force, which highlights that the total thrust could be controlled efficiently by extracting pressurized air from an optimal position in the compressor section.

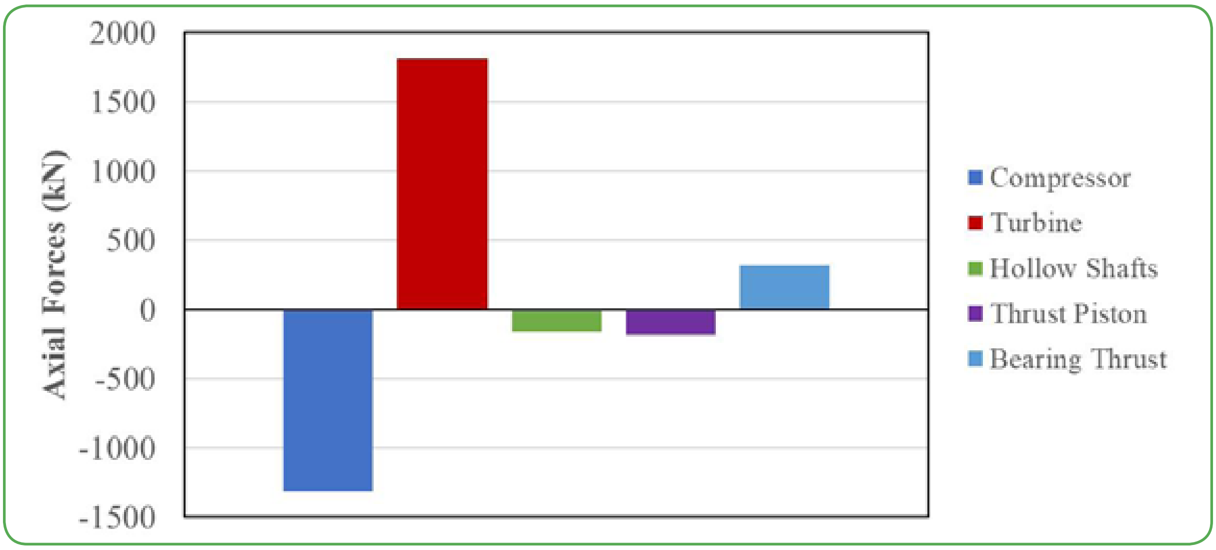

Figure 11- Thrust Calculation Results for the MGT-70 Rotor under Base-Load Conditions

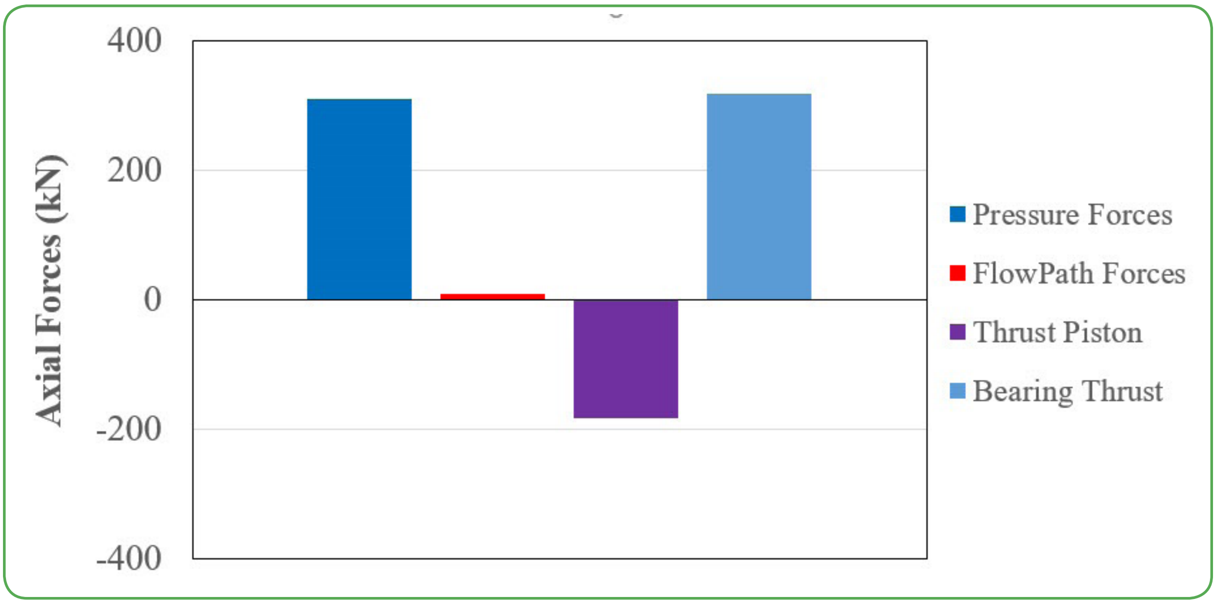

Figure 12- Thrust Distribution by the Rotor Components of the MGT-70 under Base-Load Conditions

Field Test Results

As previously described, the front housing incorporates a dual thrust-bearing arrangement comprising active and passive elements as depicted in Figure 13. The active thrust bearing incorporates nineteen pads with comparatively larger dimensions, reflecting its role in carrying the axial load during typical engine operation. In contrast, the passive thrust bearing consists of a greater number of pads of smaller size, corresponding to its function in sustaining the relatively lower reverse thrust load. For experimental characterization, two load cells were installed on a pair of active pads positioned approximately 180° apart. The thrust forces measured by these two sensors were recorded over time, and their time history is presented in Figure 14.

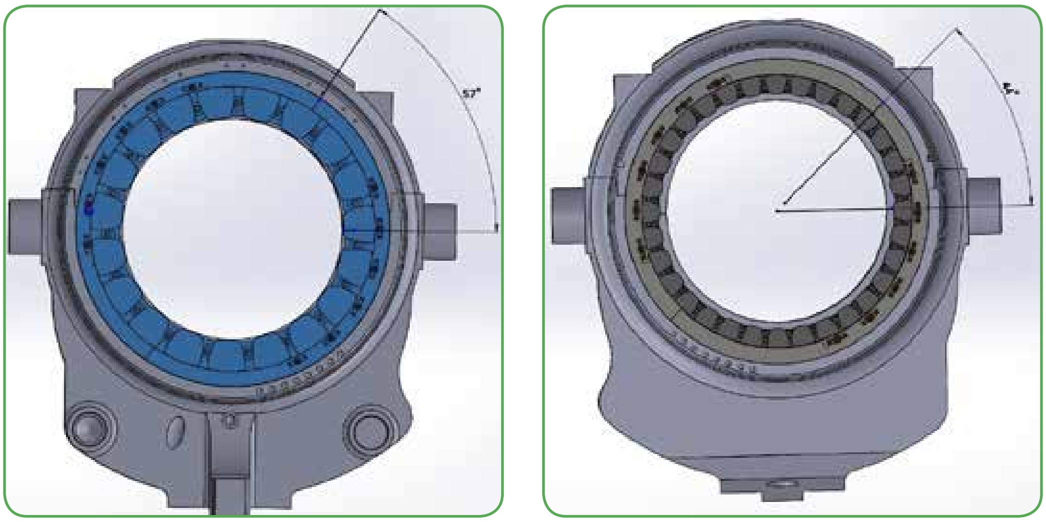

Figure 13- The Active (Left) and the Passive (Right) Thrust Bearings

As observed in the measurements, the two instrumented thrust pads experience different axial force levels under varying operating conditions. Therefore, to enable appropriate comparison between the three-dimensional numerical predictions and the experimental measurements, the mean axial load of these two pads is considered. Given that the active thrust bearing employed in this test consists of 19 pads, the total rotor thrust obtained from the experimental data for the MGT-70 turbine rotor is approximately 300 kN under base-load conditions.

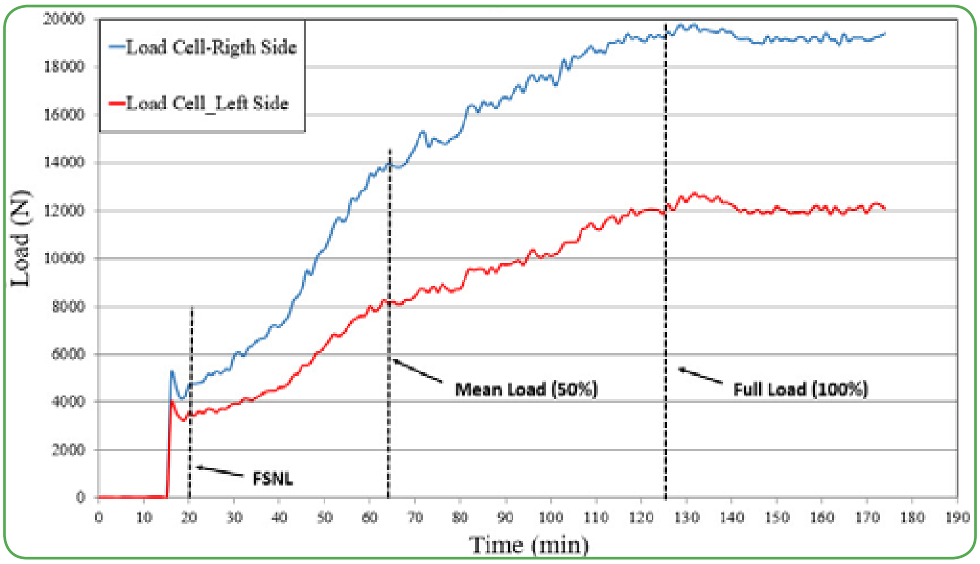

Figure 14- Measured Loads on the MGT-70 Active Thrust Bearing Pads

Figure 15 illustrates the variation of thrust as a function of gas turbine load for both the experimental measurements and the numerical predictions of the current study. Generally, a strong correlation is observed between the two datasets, confirming the capability of the proposed method.

Despite this agreement, some deviations are observed between the numerical and experimental curves. At lower loads, the numerical results predict a higher thrust level than the experimental data. This deviation can be referred to the transient behavior of engine and some other factors such as estimation of aerodynamic losses and leakage flows at partial loads, inherently present in real engine environments but are only minimally represented in numerical simulations. These phenomena may have a proportionally larger impact under part-load conditions, where component efficiencies change and tip-clearance losses become more significant. However, toward the full-load condition, the predicted thrust reaches 315 kN, slightly higher than the measured value of 305 kN. The close agreement at maximum load demonstrates that the modeling framework successfully represents normal operating conditions, where flow structures are more stable, and highlights the reliability of the numerical methodology.

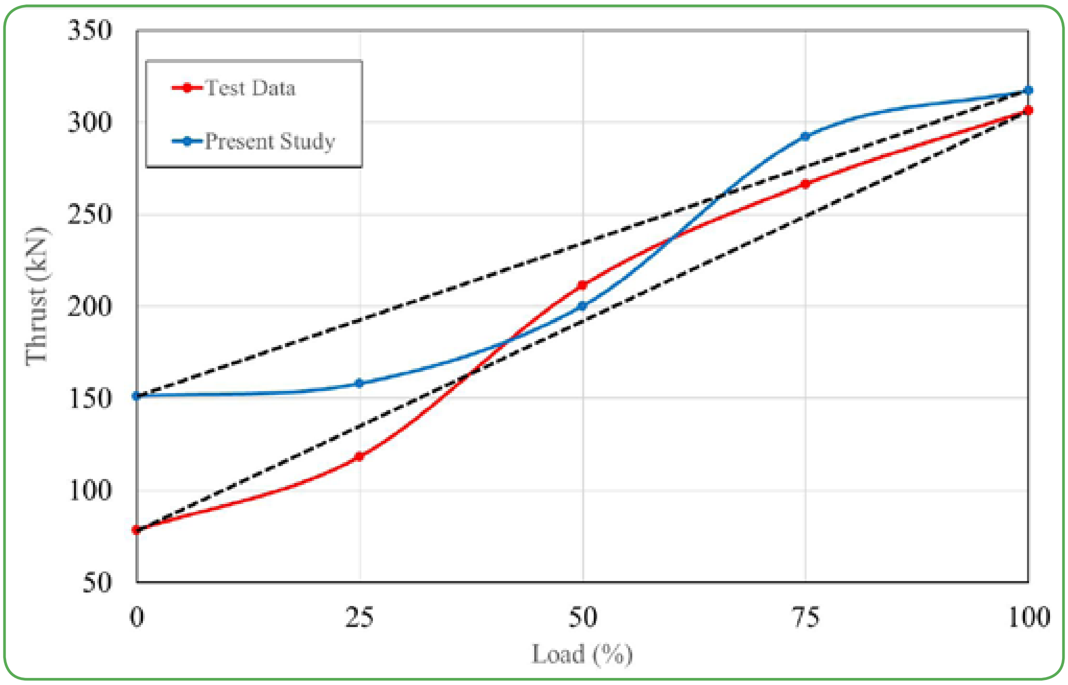

Figure 15- Comparison of Axial Thrust Obtained from 3D Simulations and Experimental Measurements

Concluding Remarks

A three-dimensional CFD methodology was developed to accurately predict rotor axial thrust in the MGT-70 gas turbine, capturing both flow path and secondary-air-induced pressure contributions. The approach integrates high-fidelity simulations of the compressor and turbine, along with detailed modeling of rotor cavities and hollow shafts, enabling precise evaluation of centrifugal-driven flows and near-wall interactions. Comparison with experimental thrust measurements shows strong agreement and validation of the method's reliability, while minor deviations at part-load highlight the transient effects. Overall, the methodology provides a robust predictive tool for thrust-bearing design, supports safe turbine operation, and reduces dependence on one-dimensional models and experimental calibration.

5

Miniature Test Methods for Characterizing Material Properties of New and Service-Exposed Components

Mousavipour, Reza
Ghorbanzade, Shabnam
MohseniZonoozi, Elnaz
Hosseini, Sedigheh

MAPNA Turbine Engineering & Manufacturing Co. (TUGA)

Introduction

Accurate evaluation of the remaining service life of turbine components is essential for ensuring the reliability, safety, and cost-effective operation of power generation systems. Components such as blades, vanes, rotors, and casings operate under extreme thermal, mechanical, and environmental conditions, which gradually induce degradation mechanisms including creep, fatigue, thermal aging, oxidation, and microstructural instability. Conventional mechanical testing methods (such as standard tensile, creep, and fracture toughness tests) provide reliable information on material condition, yet they require large specimen volumes that cannot be extracted from in-service turbine parts without causing unacceptable damage.

In response to these limitations, small scale sampling and miniature testing techniques have gained increasing attention as practical tools for life assessment programs. Scoop sampling enables extraction of a minimum amount of material from critical locations of turbine components with negligible impact on their structural integrity. The obtained samples can then be subjected to miniature mechanical tests such as small punch testing and miniature tensile testing, which offer material property estimates comparable to those obtained from conventional tests.

Given the prolonged operation of turbine components, the significant economic impact of replacement, and limited inspection opportunities, miniature testing techniques provide an effective means of assessing material degradation with minimal invasiveness. This approach combines localized sampling with advanced miniature testing methods to characterize material degradation, calibrate life prediction models, and make informed decisions regarding maintenance, repair, and replacement. This study reviews the principles of scoop sampling, miniature tensile testing and small punch testing within the context of turbine life assessment, highlighting their capabilities, limitations, and practical significance for the power generation industry.

Scoop Sampling

The application of miniature specimens for condition monitoring of aging plant components relies on the capability to extract small samples from a component or to employ portable field equipment for tests such as ball indentation directly on the component.

An in-situ sampling technique is commonly employed to remove material from operating components in a manner analogous to scooping ice cream [1].

Scoop sampling is a semi-destructive specimen extraction method that provides small material samples for further analysis of in-service components.

Although scoop sampling has been used since the late 1980s, it has gained widespread industrial acceptance only in recent years due to technological advances that have improved equipment availability, portability, and cutting speed [2].

Scoop sampling machines are designed to operate without altering the mechanical or metallurgical properties of the extracted material. Miniature specimens can be prepared from the scooped sample and subsequently tested to determine the mechanical properties of the in-service component.

Figure 1- TUGA Scoop Sampling Device

The scoop sampling device designed and manufactured by TUGA is based on the mechanical cutter principle.

This device, shown in Figure 1, incorporates a 54 mm diameter cup-shaped cutter blade coated with CBN (Figure 2). The system is capable of extracting a lens-shaped specimen with an approximate diameter of 26 mm and a depth of 3.5 mm (Figure 3).

Figure 2- Cup-Shaped Cutter Blade Coated with CBN

Figure 3- Diameter and Depth of Lens-Shaped Specimen

To date, the device has been successfully employed for the following applications:

- Sampling of new and service-exposed TBC-coated mixing chambers to evaluate coating degradation on the actual components (not test samples) with complex geometries and to investigate the influence of service conditions on the remaining coating life.
- Sampling of compressor components that have reached their design service life and require mechanical property characterization and microstructural evaluation.
- Sampling of gas turbine combustion chamber components to assess the structural degradation, characterize oxide layer thickness and morphology, and evaluate the feasibility of life extension.
- Sampling of gas turbine disks and turbine casing components to evaluate structural degradation and deterioration of mechanical properties.
- Sampling of components lacking reliable manufacturing or material documentation, where mechanical property evaluation was required to determine their suitability for continued service as structurally sound components.
- Sampling of localized regions of components that experienced damage or nonconformities during manufacturing or assembly processes, where mechanical property data were required for engineering decisions without destroying the component.

Miniature Specimen Testing

Meeting the specimen size requirements for conventional mechanical testing is not always feasible. Consequently, there is growing interest in evaluating material properties using small specimens. Small-specimen testing was first introduced in the 1970s for the characterization of materials used in nuclear reactors. Since then, Small Specimen Test Technology (SSTT) has found applications in numerous fields, including residual life assessment of in-service components in the fossil energy industry, local mechanical property measurements in welded structures, and the evaluation of the mechanical properties of miniature devices such as microelectromechanical systems (MEMS) [3-6].

Mechanical testing performed on specimens that are significantly smaller than conventional specimens is broadly referred to as miniature specimen testing.

A variety of miniature specimen testing techniques have been developed over time and can be broadly classified into two categories:

- Tests Based on Direct Scaling down of Conventional Specimen Geometries:

This category includes specimens that retain the shape and configuration of full-scale tensile, fracture toughness, fatigue, and impact specimens while their dimensions are reduced proportionally. The loading configuration remains essentially identical to that used in conventional mechanical testing. The Miniaturized Tensile Test (MTT) is one of the most widely used SSTT methods and employs specimens ranging from several millimeters to hundreds of micrometers in the minimum dimension (thickness or diameter).

- Tests Based on Unconventional Specimen Geometries and Novel Loading Techniques:

The simplest specimen configuration in this category is the disk specimen, with diameters ranging from 3 to 8 mm and thicknesses from 0.3 to 1 mm. The most common tests employing disk specimens are punch tests (shear punch and small punch tests) and spherical or ball indentation tests.

■ Miniaturized Tensile Testing

Tensile testing using sub-size specimens has the potential to provide stress–strain data representative of bulk material behavior, provided that various key factors are carefully considered. These factors include the microstructure characteristics and their relationship to specimen dimensions, specimen preparation methods, specimen alignment within the load train, resolution and accuracy of load measurements, and strain measurement techniques.

As specimen dimensions decrease, special precautions must be taken during specimen preparation and handling. The preferred method for machining sub-size tensile specimens is Electro-Discharge Machining(EDM), followed by diamond grinding and polishing to remove the recast layer and achieve the required dimensional tolerances.

At TUGA, both room-temperature and high-temperature tensile testing are routinely performed. Dedicated fixtures for both testing conditions have been designed and manufactured using materials suitable for the respective test environments.

The dimensions of the miniature tensile specimens were determined through detailed analysis and simulation of the stress distribution under loading throughout specimens of varying thicknesses. Pin-loaded specimens are prepared and tested for high-temperature applications, while pin-free specimens are used for room-temperature testing.

The room-temperature and high-temperature test fixtures are shown in Figures 4 and 5, respectively. In addition, Figure 6 shows a pin-loaded specimen before and after testing.

Figure 4- Fixture for Room-Temperature Miniature Tensile Tests

Figure 5- Fixture for High-Temperature Miniature Tensile Tests

Figure 6- Pin-Loaded Specimen before and after Testing

- **Small Punch Test (SPT)**

The Small Punch Test (SPT) evolved from the Miniature Disk Bend Test (MDBT), originally developed by Manahan et al. at the Massachusetts Institute of Technology in 1982. The principal difference between the MDBT and the SPT lies in the degree of mechanical constraint imposed on the specimen. In a standard SPT configuration, a thin disk-shaped specimen is rigidly clamped between an upper and a lower die and subjected to out-of-plane deformation by a hemispherical punch until fracture occurs. To reduce wear and improve experimental repeatability, standardized procedures such as the European Committee for Standardization (CEN) workshop agreement standard permit alternative punch configurations, including fully machined hemispherical punches or flat/concave punches used in conjunction with rigid spherical ball bearings [7].

The standardization of this methodology advanced significantly with publication of the European Code of Practice (EUCoP) for tensile, fracture, and creep testing using the Small Punch Test by CEN in 2006. This framework subsequently evolved into EN and ASTM standards, thereby promoting broader international acceptance and improving inter-laboratory reproducibility [8].

- **Practical applications of the small punch test at TUGA**

One of the critical concerns for certain cold-section turbine components during service is the degradation of material toughness. Studies have shown that the small punch absorbed energy measured at a single temperature cannot by itself reliably represent the fracture toughness behavior of a material. Instead, the Fracture Appearance Transition Temperature (FATT) is considered as a more appropriate parameter for integrity assessment and engineering decision-making.

Determination of the FATT requires testing a large number of specimens over a wide range of temperatures. However, extracting sufficient sub-size or standard specimens from scoop-sampled material is generally impractical due to the limited volume of available material. Therefore, TUGA has employed the SPT to determine the FATT of materials when only scoop samples are available.

Figure 7 illustrates the preparation of small punch specimens extracted from a gas turbine disk. Following wire-cut EDM and punching operations, the specimens were ground and polished to a final thickness of 500 µm. Multiple tests were conducted at temperatures ranging from −196°C to room-temperature using the SPT system shown in Figure 8.

Figure 7- Small Punch Specimens Extracted from a Gas Turbine Disk

Figure 8- Low Temperature Small Punch Machine

The normalized absorbed energy values and the corresponding Small Punch Transition Temperature (TSP) obtained from the test results are presented in Figure 9. According to miniature testing standards, the TSP can be correlated with the conventional FATT. In the present study, approximately 30 standard-sized specimens were extracted from the disk material and tested at various temperatures to determine the FATT directly. Comparison of the results demonstrated that the two parameters exhibited a well-defined correlation and can be converted into one another through an appropriate correlation factor.

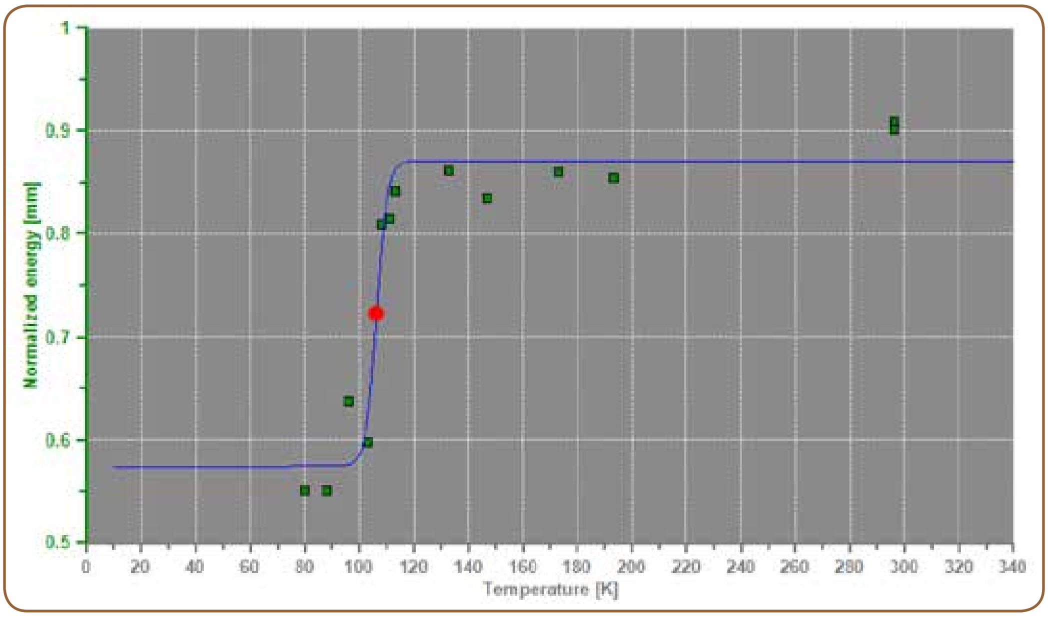

Figure 9- Small Punch Transition Temperature (TSP)

Another important application of the Small Punch Test is creep property characterization. To determine the creep properties of various materials, particularly turbine blades from which standard creep specimens cannot be extracted, TUGA has developed and tested small punch creep specimens.

Figure 10 shows the extraction of sub-size tensile, miniature tensile, and small punch specimens from a turbine blade. Creep testing of service-exposed turbine blades can provide valuable information for remaining service life assessment. Figure 11 presents the testing system used to perform small punch creep tests at temperatures of approximately 900 °C.

Figure 10- Extraction of Small Specimens from a Turbine Blade

Figure 11- High-Temperature Small Punch Machine

Concluding Remarks

The semi-destructive sampling techniques, which require no post-sampling repair and cause no significant damage to the component, alongside small-scale testing methodologies have been employed at TUGA. By employing testing methods such as miniature tensile testing at ambient and elevated temperatures, small punch creep testing, and determination of the ductile-to-brittle transition temperature via the small punch method, the material properties of both newly manufactured and in-service components can be characterized. These data, in turn, enable the reliable prediction of the remaining service life of the components.

References

[1] V. Karthik, K.V. Kasiviswanathan, and Baldev Raj *"Miniaturized Testing of Engineering Materials"*, CRC Press Taylor & Francis Group, 2017.

[2] D. Marriott, S. Read, A. Sreeranganathan, *"The use of miniature test specimen in fitness-for service evaluation"*, Inspectioneering Journal, May/June, 2016.

[3] P. Zheng, R. Chen, H. Liu, J. Chen, Z. Zhang, X. Liu, Y. Shen ,*"On the standards and practices for miniaturized tensile test – A review"*, Fusion Engineering and Design, 161 (2020).

[4] K. Kumar, A. Pooleery, K. Madhusoodana, R.N. Singh , A. Chatterjee, B.K. Dutta , R.K. Sinha ,*"Optimisation of thickness of miniature tensile specimens for evaluation of mechanical properties"*, Materials Science & Engineering A, 675(2016).

[5] T. H. Hyde1, W. Sun1 and J. A. Williams, *"Requirements for and use of miniature test specimens to provide mechanical and creep properties of materials: a review"*, International Materials Reviews, 2007 VOL 52 NO 4.

[6] K. Kumar, A. Pooleery, K. Madhusoodanan, R. N. Singh, J. K. Chakravartty, B K Dutta and R.K. Sinha, *"Use of Miniature Tensile Specimen for Measurement of Mechanical Properties"*, Procedia Engineering, 86 (2014).

[7] S. Arunkumar, *"Overview of small punch test"*, Metals and Materials International, 2020.

[8] R.J. Lancaster, et al. *"Derivation of material properties using small punch and shear punch test methods"*, Materials & Design, 2022.

MAPNA GROUP
MAPNA Turbine Engineering and Manufacturing Company

Head Office:
231 Mirdamad Ave. Tehran, I.R.Iran.
P.O.Box: 15875-5643
Tel: +98 (21) 22908581
Fax: +98 (21) 22908654

Factory:
Mapna blvd., Fardis, Karaj, I.R.Iran.
Post code: 31676-43594
Tel: +98 (26) 36630010
Fax: +98 (26) 36612734

www.mapnaturbine.com

The technical and other data contained in this Technical Review is provided for information only and may not apply in all cases.

GR697-0